

Assessing acetone for the GISS ModelE2.1 Earth system model

Alexandra Rivera¹, Kostas Tsigaridis^{2,3}, Gregory Faluvegi^{2,3}, Drew Shindell⁴

¹Pratt School of Engineering, Duke University, Durham, NC, 27708, USA

²Center for Climate Systems Research, Columbia University, 2880 Broadway, New York, NY, 10025, USA

³NASA Goddard Institute for Space Studies, 2880 Broadway, New York, NY, 10025, USA

⁴Nicholas School of the Environment, Duke University, Durham, NC, 27708, USA

Correspondence to: Kostas Tsigaridis (kostas.tsigaridis@columbia.edu)

Abstract. Acetone is an abundant volatile organic compound (VOC) in the atmosphere with important influence on ozone and oxidation capacity. Direct sources include chemical production from other VOCs as well as anthropogenic emissions, terrestrial vegetation, biomass burning emissions, and ocean production. Sinks include chemical loss, deposition onto the land surface, and ocean uptake. Acetone also has a lifetime that is long enough to allow transport and reactions with other compounds remote from its sources. The NASA Goddard Institute for Space Studies (GISS) Earth System Model, ModelE2.1, simulates a variety of Earth system interactions. Previously, acetone had a very simplistic representation in the ModelE chemical scheme. This study assesses a more sophisticated acetone scheme in which acetone is a full 3-dimensional tracer with explicit sources, sinks, and atmospheric transport. We first evaluate the new global acetone budget in the context of past literature. Estimated source and sink fluxes fall within the range of previous models, although total atmospheric burden and lifetime fall on the lower end of published literature. Acetone's new representation in the ModelE2.1 also results in more realistic spatial and vertical distributions, which we compare against previous models and field observations. The seasonality of acetone-related processes was also studied in conjunction with field measurements, and these comparisons show promising agreement but have shortcomings at high-emission urban locations where the model's resolution is too coarse to capture the behavior. Finally, we conduct a variety of sensitivity studies that explore the influence of key parameters on the acetone budget and its global distribution. An impactful finding is that the production of acetone from precursor hydrocarbon oxidation has strong leverage on the overall chemical source, indicating the importance of accurate molar yields. Overall, our implementation is one that corroborates with previous studies and marks a significant improvement to the development of the acetone tracer in the GISS ModelE2.1.

1 Introduction

Acetone (C_3H_6O) is an abundant oxygenated volatile organic compound (VOC) that has important connections to ozone and the atmosphere's self-cleansing oxidation capacity (Read et al., 2012). Acetone's dynamic presence in Earth's atmosphere can be described through sources, sinks, and mechanisms of transport. Extensive literature has discussed the nature of these sources and sinks, and some are more well-constrained than others.

Primary sources of acetone in the atmosphere include anthropogenic, terrestrial vegetation, and biomass burning emissions. Past literature has found the fluxes of these sources to range between 1-2 Tg yr⁻¹, 30-45 Tg yr⁻¹, 2.5-4.5 Tg yr⁻¹, respectively (Beale et al., 2013; Brewer et al., 2017; Elias et al., 2011; Fischer et al., 2012; Folberth et al., 2006; Jacob et al., 2002; Singh et al., 2000; Wang et al., 2020). Chemical production from other VOCs with 3 or more carbon atoms, each with their own molar yields, is another source of acetone in the atmosphere (Brewer et al., 2017; Fischbeck et al., 2017; Hu et al., 2013; Jacob et al., 2002; Singh et al., 2000; Weimer et al., 2017).

37

38 Sinks of acetone include wet and dry deposition, as well as chemical loss. Wet deposition occurs within and below clouds due to
39 the solubility of acetone, and depends on its Henry's Law coefficient (Benkelberg et al., 1995). Dry deposition occurs on the land
40 surface. Chemical loss of acetone forms radicals through photolysis. Past literature has estimated the acetone sinks to be 10-30%
41 dry deposition and 40-85% chemical loss (Arnold et al., 2005; Elias et al., 2011; Fischer et al., 2012; Khan et al., 2015; Singh et
42 al., 1994). The estimated fluxes are 10-16 Tg yr⁻¹ and 45-60 Tg yr⁻¹ for total deposition and chemical loss, respectively (Arnold et
43 al., 2005; Brewer et al., 2017; Dufour et al., 2016; Elias et al., 2011; Fischer et al., 2012; Jacob et al., 2002; Khan et al., 2015;
44 Marandino et al., 2005; Singh et al., 2000; Wang et al., 2020).

45

46 The ocean surface is a bidirectional flux that provides both a source and a sink for acetone. Ocean surface conditions such as wind
47 speed, sea surface temperature, and seawater concentration of acetone can influence the direction and magnitude of ocean-acetone
48 exchange (Wang et al., 2020). Previous literature estimates an oceanic source flux of 25–50 Tg yr⁻¹ and oceanic uptake flux of
49 35–60 Tg yr⁻¹. However, there is little consensus in the literature on whether the ocean serves as a net source or sink of acetone,
50 with some studies indicating a net oceanic source (Beale et al., 2013; Jacob et al., 2002; Wang et al., 2020), and other studies
51 indicating a net oceanic sink (Brewer et al., 2017; Elias et al., 2011; Fischer et al., 2012; Wang et al., 2020).

52

53 In addition to a global annual mean atmospheric budget, previous studies have reported the seasonality of acetone-related processes.
54 Past studies have compared monthly estimates of acetone mixing ratios to field measurements of European sites from Solberg et
55 al. (1996) (Arnold et al., 2005; Elias et al., 2011; Jacob et al., 2002). Comparisons with these European sites have emphasized the
56 seasonal variability of acetone emissions, as nearly all sites portray a summer maximum and winter minimum of acetone
57 abundance. Vegetation emissions from June to September, along with chemical sources, have an especially strong contribution to
58 this seasonality. The winter minimum of acetone is aided by an ocean sink at coastal sites (Jacob et al., 2002).

59

60 Other studies have described spatial distributions and seasonal dependence of ocean fluxes of acetone (Fischer et al., 2012; Wang
61 et al., 2020). A model by Fischer et al. (2012) proposed a net ocean sink of 2 Tg yr⁻¹ and characterized ocean uptake of acetone as
62 strongest in northern latitudes year-round and in the high southern latitudes during the winter. An oceanic acetone source was
63 dominant in the tropical regions, with an exception off the western coasts of Central America and Central Africa (Fischer et al.,
64 2012). A model by Wang et al. (2020) that varied surface seawater acetone concentration through a machine learning approach
65 also proposed a net ocean sink year-round. This net sink was strongest in December-February, and weakest in March-May.

66

67 The vertical distribution of acetone has been modeled between the seasons of May-October and November-April in the surface
68 and troposphere (Fischer et al., 2012). Acetone concentrations are generally higher in the lower altitudes due to proximity to surface
69 emissions. Surface-level acetone has been measured over a variety of terrestrial and oceanic sites around the world (de Gouw et
70 al., 2004; Dolgorouky et al., 2012; Galbally et al., 2007; Guérette et al., 2019; Hu et al., 2013; Huang et al., 2020; Langford et al.,
71 2010; Lewis et al., 2005; Li et al., 2019; Read et al., 2012; Schade and Goldstein, 2006; Singh et al., 2003; Solberg et al., 1996;
72 Warneke and de Gouw, 2001; Yoshino et al., 2012; Yuan et al., 2013), and in some cases, these measurements were taken over a
73 variety of months to provide a sense of seasonality (Dolgorouky et al., 2012; Hu et al., 2013; Read et al., 2012; Schade and
74 Goldstein, 2006; Solberg et al., 1996). Additionally, vertical distributions of acetone have been measured through NASA's
75 Atmospheric Tomography Mission (ATom) campaigns (Thompson et al., 2022). The ATom-1, ATom-2, ATom-3, and ATom-4
76 campaigns took place during July-August 2016, January-February 2017, September-October 2017, and April-May 2018,

77 respectively. Each campaign provided mixing ratios for a variety of VOCs in profiles from the marine boundary layer up to the
78 upper troposphere/lower stratosphere (Apel et al., 2021).

79
80 The NASA Goddard Institute for Space Studies (GISS) ModelE2.1 Earth System Model (Kelley et al., 2020) has the capability of
81 simulating a variety of Earth system interactions, is used both to interpret and predict past and future climate, and routinely
82 participates in the Climate Model Intercomparison Projects (CMIP) and Intergovernmental Panel for Climate Change (IPCC)
83 reports. Here we used and enhanced this model by adding acetone as an independent chemical tracer (Kelley et al., 2020).
84 Previously, acetone had a very simplistic representation in the model's chemical scheme (Shindell et al., 2003), in which acetone's
85 spatial variation was parameterized based on the difference of the model's zonal mean distribution of isoprene and that tracer's
86 three-dimensional distribution. Acetone's lifetime is long enough to be transported remote from sources, but not long enough to
87 become uniformly mixed, and therefore its simulated distribution should benefit from a more realistic implementation. We
88 developed a greatly improved acetone tracer scheme by making prognostic calculations of the 3-dimensional distribution of acetone
89 as a function of time. We evaluated its atmospheric burden and lifetime as well as source/sink fluxes (anthropogenic emissions,
90 vegetation emissions, biomass burning, deposition, ocean, and chemistry) against other models and its concentration against field
91 measurements. This work aims to provide a holistic assessment of the abundance of acetone in the atmosphere.

92 **2 Methodology**

93 Here we implement acetone in the GISS ModelE2.1 based on the literature rather than developing a new parameterization. Our
94 'Baseline' simulation is a climatological mean with year 2000 conditions, chosen to be relatively modern without precluding
95 comparison with models in older literature. The 1996-2004 mean of prescribed emissions from Hoesly et al. (2018) were used,
96 along with the 1996-2005 mean sea surface temperature and sea ice cover as described in Kelley et al. (2020). Acetone simulations
97 use full chemistry and not archived OH fields. An additional simulation, 'Nudged_ATOM', was conducted to compare more directly
98 with ATom field measurements. This simulation employed nudged winds from MERRA2 (Gelaro et al., 2017), ocean surface
99 conditions from PCMDI-AMIP 1.1.4 for 2016-2017 (Taylor et al., 2000) and from Hadley Center HadISST1.1 for 2018 (Met
100 Office, Hadley Centre, 2006), and trace gas and aerosol emissions changing with time during 2016-2018.

101 **2.1 Sources**

102 **2.1.1 Anthropogenic emissions**

103 Anthropogenic emissions were prescribed using the 1996-2004 averages of the Community Emissions Data System (CEDS)
104 emissions from Hoesly et al. (2018) as prepared for the GISS contributions to the Coupled Model Intercomparison Project, Phase
105 6 (CMIP6) (Kelley et al., 2020). These include sources from agriculture, the energy sector, the industrial sector,
106 residential/commercial/other, international shipping, solvents production and application, the transportation sector, and waste. In
107 line with past studies, we base acetone emissions on that of ketones. VOC23-ketones emissions from Hoesly et al. (2018) were
108 scaled down by a ratio of acetone molecular weight to an average ketone molecular weight ($58.08 \text{ g mol}^{-1}/75.3 \text{ g mol}^{-1}$).
109 Maintaining the resulting spatial and temporal pattern of emissions, the magnitudes were then tuned to be close to that of Fischer
110 et al. (2012), resulting in a total of about 1 Tg yr^{-1} . This resulted in roughly 36.5% of CEDS VOC23-ketones used as acetone
111 emissions. Lacking an accurate way to obtain acetone aircraft emissions from the bulk VOCs available in the emission inventory,
112 we have neglected that sector in the simulations.

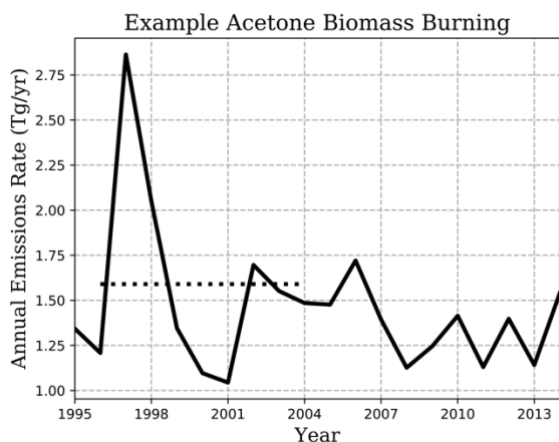
113 2.1.2 Terrestrial vegetation emissions

114 Emissions from land vegetation were derived from the Model Emissions of Gases and Aerosols from Nature (MEGAN), version
115 2.1 (Guenther et al., 2012), a new contribution to the ModelE. Emission response algorithms in the MEGAN2.1 model are derived
116 from input leaf area indices, solar radiation, temperature, moisture, CO₂ concentrations, and plant functional types and composition
117 of species (Guenther et al., 2012). The acetone vegetation emissions in the Baseline simulation in GISS ModelE2.1 were calculated
118 to equal 36.1 Tg yr⁻¹.

119 2.1.3 Biomass burning emissions

120 Acetone emissions were prescribed from a 1996-2004 average of the NMVOC-C₃H₆O species from version 2.1 of the biomass
121 burning dataset of van Marle et al. (2017), used by CMIP6. The acetone mass flux from biomass burning in the Baseline simulation
122 was 1.59 Tg yr⁻¹.

123
124 Figure 1 shows the biomass burning emission rate chosen for this study, and how it lies within the range of substantial interannual
125 variation. During the 20-year period shown, emissions averaged 1.46 Tg yr⁻¹, with a standard deviation of 0.402, and a spike in the
126 earlier years of emissions over 2.75 Tg yr⁻¹ is also observed (Figure 1). On top of any differences across emission inventories, the
127 years considered when reporting emissions may be the reason for disagreements between models (e.g. 2.40 – 2.80 Tg yr⁻¹ from the
128 2006 GFED-v2 emission inventory in Elias et al. (2011) and Fischer et al. (2012), compared to 3.22 Tg yr⁻¹ from 1997-2001 in
129 Folberth et al. (2006)).



130
131 **Figure 1.** Illustration of interannual variation of NMVOC-C₃H₆O biomass burning emissions of van Marle et al. (2017) (solid
132 line), used as acetone emissions in our simulation. Climatological-emissions simulations use the 1996-2004 mean (dotted line),
133 though emissions vary by month.

134 2.2 Sinks

135 2.2.1 Deposition

136 Both dry and wet deposition of acetone were included in the model, although dry deposition was, on average, 91% of total
137 deposition. The wet deposition scheme is given by Koch et al. (1999). Acetone and other species are transported within and below
138 clouds, and soluble gases are deposited depending on the conditions of the grid box they are in and a Henry's Law Coefficient
139 (Shindell et al., 2001). The Henry's Law Coefficient for acetone used in the GISS ModelE2.1 is 27 mol L⁻¹ atm⁻¹, with a Henry
140 temperature dependence of acetone of 5300 J mol⁻¹ (Benkelberg et al., 1995; Zhou and Mopper, 1990). The dry deposition scheme

141 uses resistance-in-series calculations, global seasonal vegetation data (Chin et al., 1996; Shindell et al., 2001; Wesely and Hicks,
142 1977), and a reactivity factor of $f_0=0.1$. This resulted in an acetone deposition rate in the Baseline simulation of 22.2 Tg yr^{-1} .

143 2.3 Chemistry

144 The GISS ModelE2.1 Baseline simulation estimates a net chemistry flux of -20.6 Tg yr^{-1} . The components can be broken up into
145 sources and sinks as follows.

146 2.3.1 Chemical sources

147 The Baseline simulation estimates chemical production to be 33.3 Tg yr^{-1} . The acetone chemical scheme includes two production
148 reactions:



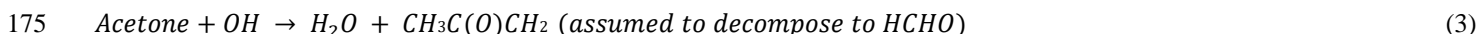
151 In the first reaction, acetone is produced by paraffin, a proxy tracer for paraffinic (saturated) carbon, and OH (Eq. 1). The molar
152 yield of acetone from paraffin was found to be a strong leverage to the overall chemical source (see Section 3.5). A rate coefficient
153 of $8.1 \times 10^{-13} \text{ cm}^3 \text{ molecule}^{-1} \text{ s}^{-1}$ was used (Shindell et al., 2003). Previous literature has suggested an acetone yield on a molecular
154 scale of 0.72 (Fischbeck et al., 2017; Jacob et al., 2002; Weimer et al., 2017). Initial tests using a yield of 0.72 resulted in an
155 overestimated chemistry source, leading us to re-evaluate this yield for the specific mixture of VOCs represented in the GISS
156 ModelE2.1.

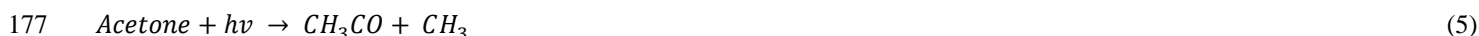
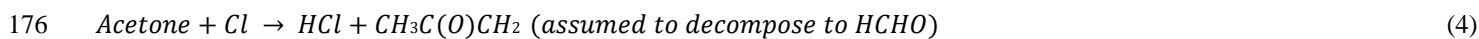
157 Our model's anthropogenic emissions of paraffin is based on an aggregation of selected VOC groups. Based on year 2019 emissions
158 of the O'Rourke et al. (2021) dataset, we emit paraffin that is about 11% propane by mole, 22% butane and 21% pentane.
159 Multiplying these by each VOC's acetone molar yield (0.73, 0.95, 0.63, respectively), we estimate that 42% of paraffin from
160 anthropogenic sources becomes acetone in our model. Paraffin biomass burning emissions, estimated from year 2020 of SSP3_70
161 emissions (Riahi et al., 2017; Fujimori et al., 2017) contain mole fractions for propane of 9% and higher alkanes of 23%, and when
162 multiplied by acetone molar yields of 0.73 and 0.79, respectively, suggest that about 25% of paraffin from biomass burning sources
163 becomes acetone in our model. The molar yields used in these calculations were derived with suggestions from the literature
164 (Fischbeck et al., 2017; Jacob et al., 2002; Weimer et al., 2017). Refer to the "Chemical sources" section of the manuscript
165 supplement for a more detailed breakdown. Overall, an average of the 42% anthropogenic paraffin and 25% biomass burning
166 paraffin was used to conclude that approximately 35% of paraffin from emissions becomes acetone, leading to our refinement of
167 the molar yield in Eq. (1) to 0.35.

168 Additionally, reactions between terpenes and $\{\text{OH}, \text{O}_3\}$ were implemented with an acetone yield of 0.12 (Hu et al., 2013; Jacob et
169 al., 2002) (Eq. 2). The rates for these reactions are $2.51 \times 10^{-11} e^{(444/T)} \text{ cm}^3 \text{ molecule}^{-1} \text{ s}^{-1}$ for the OH reaction and $1.40 \times 10^{-14} e^{(-732/T)}$
170 $\text{ cm}^3 \text{ molecule}^{-1} \text{ s}^{-1}$ for the O_3 reaction, and these coefficients are enhanced from the standard α -pinene one to consider the reactivity
171 variability across mono- and higher terpenes (Tsigaridis and Kanakidou, 2003).

172 2.3.2 Chemical sinks

173 The chemical sink of acetone in the Baseline simulation is estimated to be 53.8 Tg yr^{-1} . The sinks of acetone include oxidation by
174 OH and Cl radicals, and photolysis:





179 The first and second acetone destruction reactions above have rates of $1.33 \times 10^{-13} + 3.82 \times 10^{-11} e^{(-2000/T)}$ $cm^3 \text{ molecule}^{-1} s^{-1}$ and
180 $7.70 \times 10^{-11} e^{(-1000/T)}$ $cm^3 \text{ molecule}^{-1} s^{-1}$, respectively (Sander et al., 2011) (Eq. 3, 4). Previously, acetone photolysis (which only
181 affected production of radicals and not acetone itself) did not utilize the model's photolysis scheme but was parameterized solely
182 as a function of orbital geometry and atmospheric pressure. In the model updates, photolysis now consists of two separate reactions,
183 where acetone forms either $CH_3CO + CH_3$ radicals or two CH_3 radicals and CO (Eq. 5, 6). The spectroscopic data used for acetone
184 photolysis is from JPL 2010 (Sander et al., 2011) and mapped onto Fast-J version 6.8d's wavelength intervals (Neu et al., 2007).
185 The photolysis cross section for Eq. 5 is pressure-dependent while that of Eq. 6 is temperature-dependent, leading to variation in
186 yields with altitude and location. For example, in a standard atmosphere the ratio of the yield of CO to CH_3CO decreases from
187 0.28 at the surface to 0.18 at 4 km altitude.

188 2.4 Ocean

189 Bidirectional fluxes of acetone are calculated over ocean based on the "two-phase" model of molecular gas exchange at the air-sea
190 interface of Liss & Slater (1974), as it is described in Johnson (2010). The fluxes are a function of simulated surface temperature
191 and near-surface wind speed but independent of salinity. Henry's Law constants and temperature dependence of solubility for
192 acetone are from Sander (1999). The source from ocean water and sink from the atmosphere are calculated assuming a constant
193 concentration of acetone in water (of 15 nM), the lower boundary layer atmospheric concentration, and the total transfer velocity
194 (a combination of water-side and air-side transfer velocities). The constant concentration of 15 nM follows the implementation by
195 Fischer et al. (2012) in the GEOS-CHEM model, who looked at observations and did not find a strong reasoning to make the
196 concentration vary seasonally or spatially. The GISS ModelE2.1 Baseline simulation calculates the ocean to be a net source of
197 acetone, producing 3.94 Tg yr^{-1} .

198 2.5 Sensitivity studies

199 Sensitivity studies were conducted to determine the influence of key parameters on the acetone budget and its global distribution
200 (summarized in Table 1). Specifically, we were interested in seeing the sensitivity of simulated acetone to artificial perturbations
201 in given parameters. Sensitivity studies for chemistry modify the production of acetone. The Chem_Cl0 and Chem_Terp0
202 simulations provide no formation of acetone from chlorine or terpenes, respectively. The importance of paraffin is explored by
203 halving its yield of acetone to 17.5% in the Chem_Par0.5 simulation, and by doubling its yield of acetone to 70% in the
204 Chem_Par2.0 simulation. As vegetation was the most prominent source of acetone, the Veg_0.7 simulation observes its reduction
205 by decreasing the MEGAN production of acetone by 30%. The Ocn_2.0 simulation aims to explore the impact of ocean acetone
206 concentration by doubling it from 15 nM to 30 nM globally. The Dep_f00 simulation tests dropping the reactivity factor for dry
207 deposition from 0.1 to 0. Finally, given the high interannual variability of biomass burning emissions, the BB_2.0 simulation
208 explores the impact of doubling those emissions.

209
210 **Table 1.** Sensitivity studies conducted to observe the leverage that a specific parameter afforded the model. Simulation names, as
211 well as the parameter they target and a description, are included.

GISS ModelE2.1 Sensitivity Simulation	Sensitivity Parameter	Description
Chem_Cl0	Chemistry Source	Acetone + Chlorine reaction rate = 0
Chem_Terp0	Chemistry Source	No reaction for production of acetone from terpenes
Chem_Par0.5	Chemistry Source	Half the yield of acetone from paraffin (17.5%)
Chem_Par2.0	Chemistry Source	Double the yield of acetone from paraffin (70%)
Veg_0.7	Vegetation	0.7 factor of acetone from MEGAN
Ocn_2.0	Ocean	Ocean acetone concentration from 15nM to 30nM
Dep_f0	Dry Deposition	f ₀ changed from 0.1 to 0
BB_2.0	Biomass Burning	Double biomass burning emissions

212 3 Results and model evaluation

213 3.1 Global acetone budget and burden

214 A global acetone budget table was compiled to place our estimates in context with past global modeling studies (Table 2) (Arnold
215 et al., 2005; Beale et al., 2013; Brewer et al., 2017; Dufour et al., 2016; Elias et al., 2011; Fischer et al., 2012; Folberth et al., 2006;
216 Guenther et al., 2012; Jacob et al., 2002; Khan et al., 2015; Marandino et al., 2005; Singh et al., 2000, 2004; Wang et al., 2020).
217 The values of the individual fluxes in our model (global deposition, biomass burning, anthropogenic emissions, vegetation
218 emissions, ocean net/source/sink, and chemistry net/source/sink) were mentioned previously.

219

220 **Table 2.** Global acetone budget table comparing burden, flux and lifetime estimates of acetone from the Baseline model to thirteen
221 previous studies.

	This Study – Baseline [2021]	Wang et al. [2020] ^a	Wang et al. [2020] ^b	Brewer et al. [2017]	Fischer et al. [2012]	Elias et al. [2011]	Jacob et al. [2002]	Other Estimates [2000-2016] ^c
Burden (Tg)	2.93	3.50	3.80	5.57	5.60	7.20	3.80	3.50 – 4.20
Global Deposition (Tg yr ⁻¹)	22.2	25.2	12.4	12.4	12.0	19.0	9.00	6.00 – 26.0
Biomass Burning (Tg yr ⁻¹)	1.59	4.00	2.40	2.60	2.80	2.40	4.50	3.22 – 9.00
Anthro Emissions (Tg yr ⁻¹)	1.00	0.50	3.40	3.60	0.73	1.60	1.10	1.02 – 2.00
Vegetation Emissions (Tg yr ⁻¹)	36.1	39.8	32.2	37.1	32.0	76.0	35.0	15.0 – 56.0
Net Ocean (Tg yr ⁻¹)	3.94	-8.10	1.30	-7.50	-2.00	-8.00	13.0	4.00
Ocean Source (Tg yr ⁻¹)	15.2	33.4	45.7	51.8	80.0	20.0	27.0	20.0
Ocean Sink (Tg yr ⁻¹)	11.3	41.5	44.4	59.2	82.0	28.0	14.0	62.0
Net Chemistry (Tg yr ⁻¹)	-20.5	-11.1	-26.1	-22.5	-21.0	-53.0	-45.0	-(5.50 – 33.0)
Chem Source (Tg yr ⁻¹)	33.3	38.5	26.1	24.1	31.0	27.0	28.0	15.5 – 55.6
Chem Sink (Tg yr ⁻¹)	53.8	49.6	52.2	46.6	52.0	80.0	73.0	33.4 – 61.1

Chemical Lifetime (days) ^c	19.9	25.8	26.6	43.6	39.3	32.9	19.0	20.9 – 35.6
Lifetime (days) ^d	12.3	11.0	12.7	17.2	14.0	21.0	14.5	12.8 – 35.0

^a CAM-Chem Model (Wang et al., 2020)

^b GEOS-Chem Model (Wang et al., 2020)

^c Chemical Lifetime = Burden/Chemical Sink

^d Total Atmospheric Lifetime = Burden/Total Sink

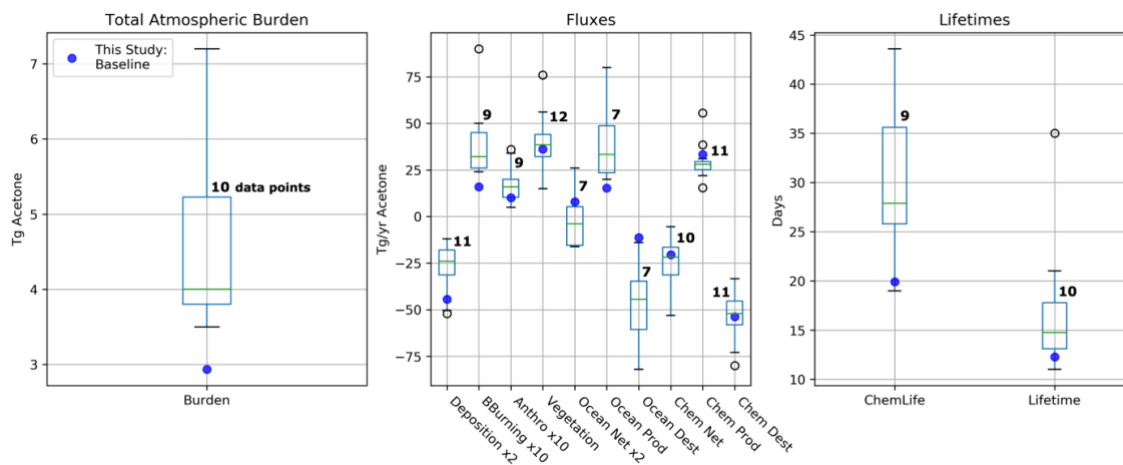
^e Singh et al. [2000, 2004], Arnold et al. [2005], Folberth et al. [2006], Marandino et al. [2006], Guenther et al. [2012], Beale et al. [2013], Khan et al. [2015], Dufour et al. [2016].

222

223 Atmospheric burden describes the total amount of acetone that is in the atmosphere. The GISS ModelE2.1 Baseline simulation
 224 estimates the burden to be 2.93 Tg. Additionally, chemical lifetime and atmospheric lifetime can be derived from burden. The
 225 chemical lifetime of acetone is calculated as the burden divided by the chemical sink, whereas total lifetime is the burden divided
 226 by all sinks. The chemical and total atmospheric lifetimes for the Baseline simulation are calculated to be 19.9 and 12.3 days,
 227 respectively. These values are also placed in the context of previous literature in Table 2.

228

229 The GISS ModelE2.1 Baseline acetone budget is further compared to previous model studies in Figure 2. The calculated fluxes in
 230 the Baseline simulation that are less than one standard deviation away from the literature mean include anthropogenic and
 231 vegetation emissions, net ocean, net chemistry, chemical production, and chemical destruction (Figure S1). Biomass burning in
 232 GISS ModelE2.1 appears as an outlier when compared against 9 previous model studies but can be attributed to the high interannual
 233 variation with emissions (as discussed in Section 2.1.3). The value of acetone deposition is on the high (more negative) end in
 234 GISS ModelE2.1 relative to 11 previous studies. This might be partially attributed to differences in deposition parametrization
 235 across models, as explored by our sensitivity study on dry deposition presented in Section 3.5.2. The values for oceanic acetone
 236 sources and losses are smaller (in absolute values) than the mean from 7 previous model studies. Nevertheless, the net ocean flux
 237 matches the literature well. Lastly, the total atmospheric burden and lifetime calculated by GISS ModelE2.1 are lower than the
 238 previous papers, an expected consequence of the higher removal by deposition. The chemical lifetime is also calculated to be at
 239 the low end of published literature.

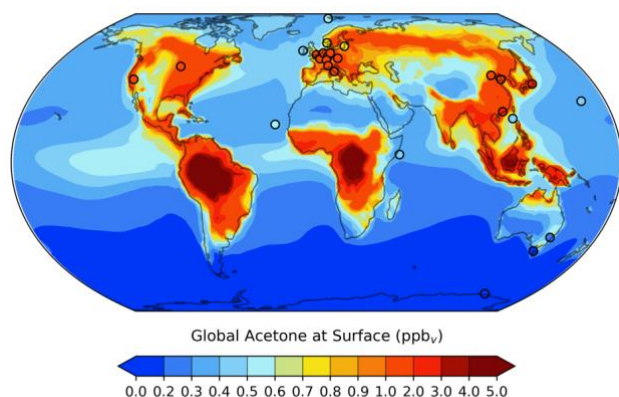


240

241 **Figure 2.** Total atmospheric burden, fluxes, and lifetimes of acetone from the literature values in Table 2 (shown in boxes and
 242 whiskers with outliers as open circles), and values from GISS ModelE2.1 (shown as solid blue circles). The number of models
 243 used to create each box and whisker plot are labeled. Note that the deposition and ocean net fluxes were multiplied by 2 and that
 244 the biomass burning and anthropogenic emissions were multiplied by 10 for a better visualization of the distribution.

245 3.2 Spatial distribution of acetone

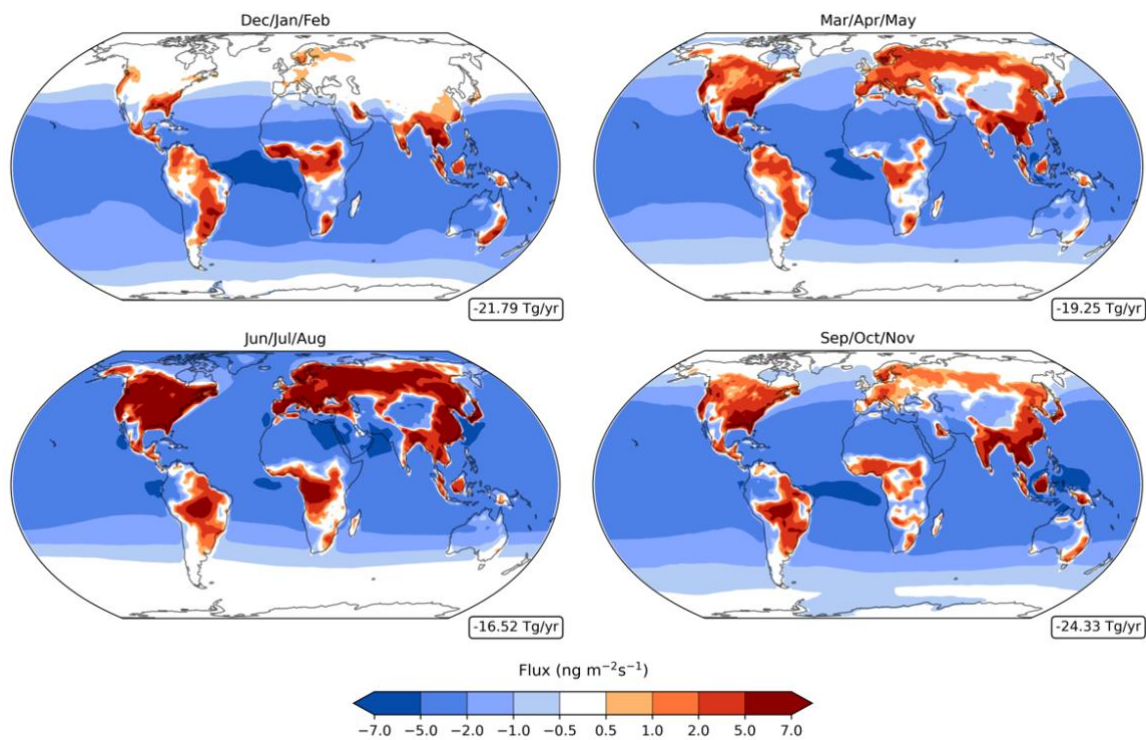
246 The global distribution of acetone at the surface is given in Figure 3. It is evident that acetone mixing ratios are largest over the
247 continents, where anthropogenic, vegetation, and other terrestrial sources are located. Over the ocean, acetone mixing ratios are
248 highest downwind of Central America and Central Africa. A comparison of the GISS ModelE2.1 results against twenty-six prior
249 field measurements shows an overall great agreement, with a root mean squared error of 0.3494 and an R^2 value of 0.8306. To put
250 these results into the context of model evaluation, a similar comparison to field measurements was done for the model's previous
251 acetone scheme. The prior parameterization was designed as a rough representation of acetone oxidized from isoprene in the upper
252 troposphere, without regard for realism near the surface, and this is evident from the comparison with surface observations: a root
253 mean squared error and R^2 value of 1.3620 and 0.0413, respectively. The improvement of the new acetone tracer model in the
254 GISS ModelE2.1 is evident from these statistics.



255 **Figure 3.** GISS ModelE2.1 spatial distribution of annual mean acetone at surface for the Baseline simulation. Filled circles
256 represent data from twenty-six field measurements (de Gouw et al., 2004; Dolgorouky et al., 2012; Galbally et al., 2007; Guérette
257 et al., 2019; Hu et al., 2013; Huang et al., 2020; Langford et al., 2010; Lewis et al., 2005; Li et al., 2019; Read et al., 2012; Schade
258 & Goldstein, 2006; Singh et al., 2003; Solberg et al., 1996; Warneke & de Gouw, 2001; Yoshino et al., 2012; Yuan et al., 2013).
259 The root mean squared error and the R^2 value between the Baseline acetone estimations and the field measurements are 0.3494
260 and 0.8306, respectively. A nonlinear colorbar is used to better differentiate the details in the map.

262 A breakdown of the acetone bidirectional fluxes indicates that its chemical production is concentrated over the continents, while
263 chemical destruction is primarily over the oceans (Figure 4). Hotspots of production over the continents include the Southeastern
264 United States and Central South America, East and Northern Asia, and Central Africa. Chemical sinks over the oceans are stronger
265 in the tropics than in the high southern or northern latitudes. Annually, there is a net flux of about $-20.46 \text{ Tg yr}^{-1}$. Observing the
266 chemical flux across all four seasons, the net loss appears unaffected while the net source changes more significantly, following
267 the seasonality of precursor compounds like isoprene and terpenes (Figure 4). Chemical production is strongest in the months of
268 June/July/August, primarily in North America and Northern Asia. Production is weakest in the months of
269 December/January/February, losing almost all production in North America and Northern Asia entirely. Still, a net negative flux
270 is present for all four seasons (Figure 4).

272



273

274

275

276

277

278

Figure 4. Net acetone chemistry fluxes (column-integrated) in the Baseline simulation for December-February (top left), March-May (top right), June-August (bottom left), and September-November (bottom right), with red indicating a net source and blue indicating a net sink. Nonlinear colorbars are used to better differentiate the details in the map. The weighted global means of the net chemistry fluxes are shown in boxes on the lower right of each subplot.

279

280

281

282

283

284

285

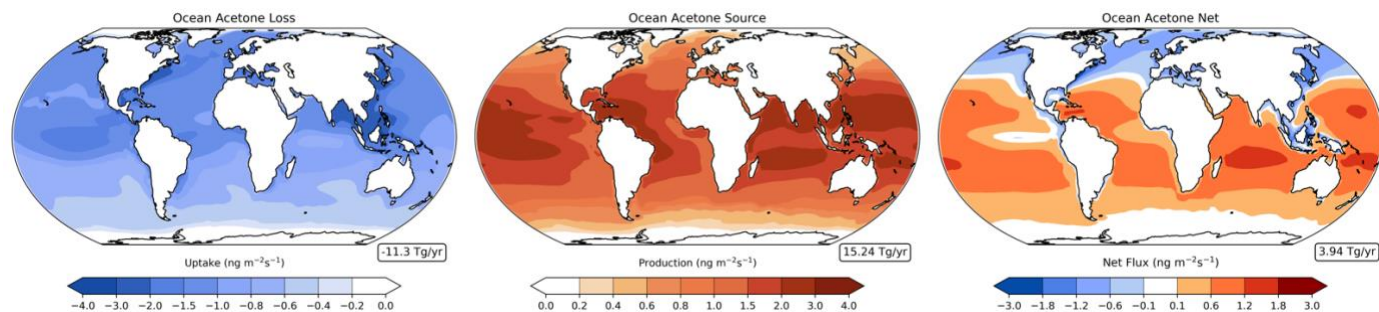
286

287

288

289

The ocean acetone sources and sinks are unevenly distributed across latitudes (Figure 5). Oceanic uptake of acetone is mostly concentrated in the northern rather than the southern oceans, while the ocean acetone source is strongest in the tropics and decreases at higher latitudes of both hemispheres. Combining these two unidirectional fluxes results in the ocean serving as a sink in the northern high latitudes, a source in the tropical latitudes, and near neutral at the high southern latitudes (Figure 5). This finding corroborates very well with findings from Fischer et al. (2012) and Wang et al. (2020). Additionally, oceanic bidirectional fluxes of acetone present trends over the four seasons (Figure S2). Overall, every season has a positive global mean net flux. However, production becomes strongest in the months of December through May, and weakest in the months of June through November. Off the coast of western South America, the ocean appears to be a net sink of acetone, even though this latitude band is generally a source of acetone (Figure 5, Figure S2). This is especially evident in the months of June/July/August and September/October/November. As the model simulates this location to have high levels of acetone at the surface (Figure 3), we believe the acetone in the air is driving the ocean to be a sink there.

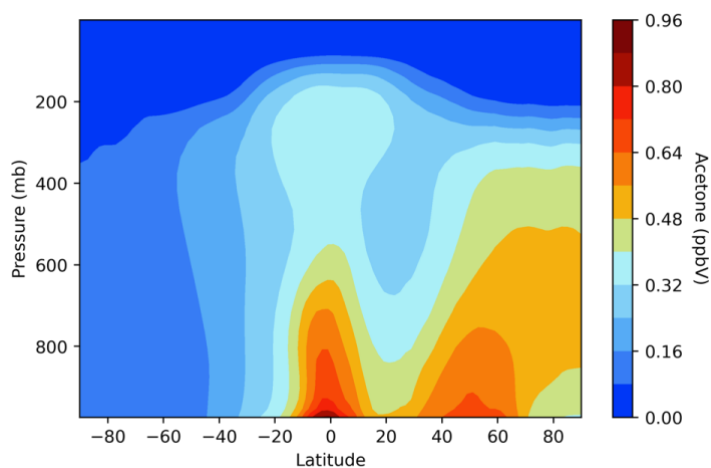


290

291 **Figure 5.** Annual mean oceanic acetone uptake (left), oceanic acetone production (middle), and net bidirectional flux (right) in the
292 Baseline simulation, with red indicating a net source and blue indicating a net sink. Nonlinear colorbars are used to better
293 differentiate the details in the map. The corresponding weighted global means of the ocean fluxes are shown in boxes on the lower
294 right of each subplot.

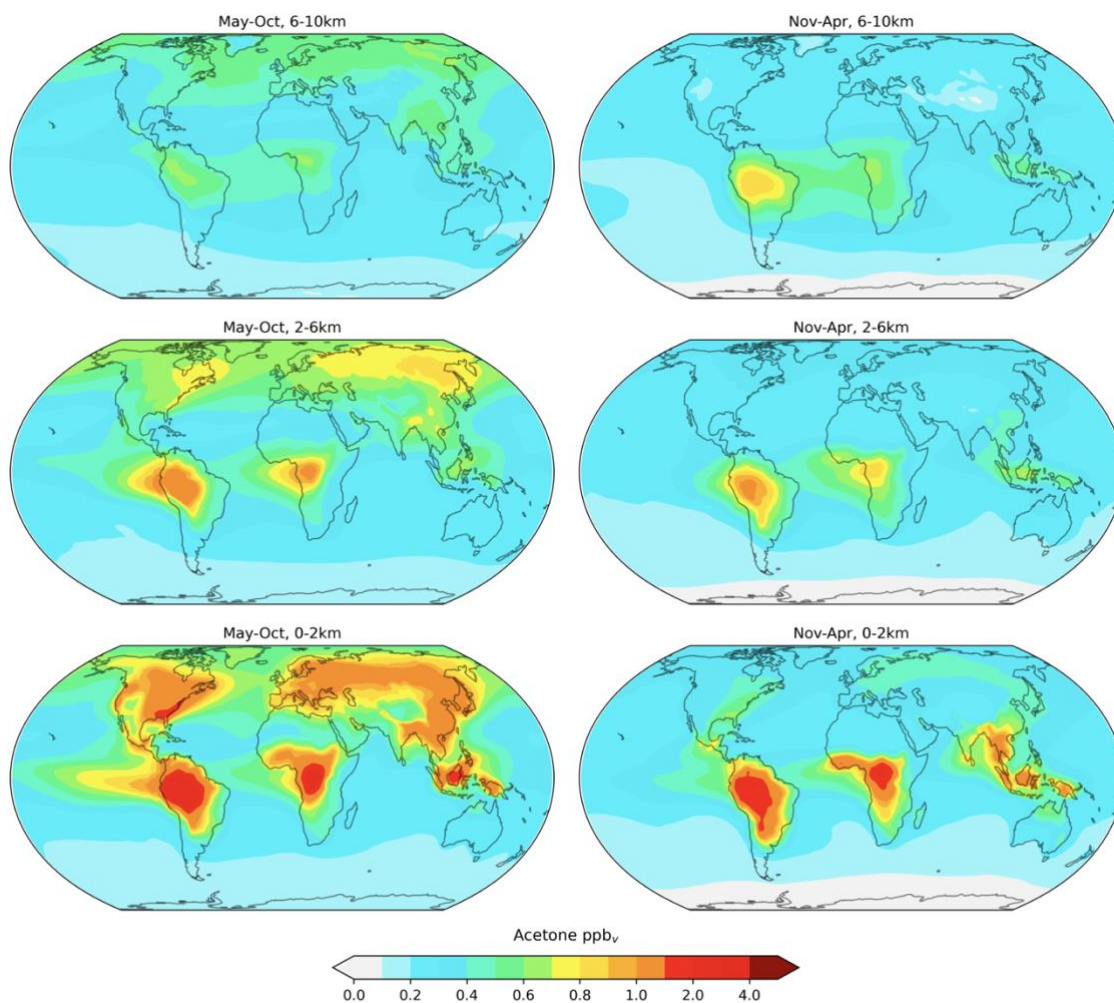
295 3.3 Vertical distribution of acetone

296 The vertical distribution of acetone varies by latitude, with near-surface air mixing ratios being higher in the tropics and in the
297 northern midlatitudes (Figure 6). Acetone levels in the atmosphere decrease with height, a direct result of sinks dominating the
298 sources. Prior to the implementation of an acetone tracer in the GISS ModelE2.1, when acetone was derived from the zonal mean
299 of isoprene, the vertical distribution looked very different. Acetone was only concentrated around the tropics and did not extend
300 nearly as high into the troposphere. The complexity of Figure 6 supports the new acetone tracer scheme as a significant
301 improvement to the GISS ModelE.



302 **Figure 6.** GISS ModelE2.1 vertical distribution of acetone air mixing ratios across latitudes in the Baseline simulation.
303

304
305 Another modeled vertical distribution of acetone, including a differentiation between two long seasons, is explored in Figure 7. In
306 general, it was found that acetone mixing ratios are higher in the months of May-October than in November-April, and that this
307 relationship is stronger in the lower atmosphere (0-2 km) than the upper atmosphere (6-10 km). This finding corroborated well
308 with a similar analysis done by Fischer et al. (2012).

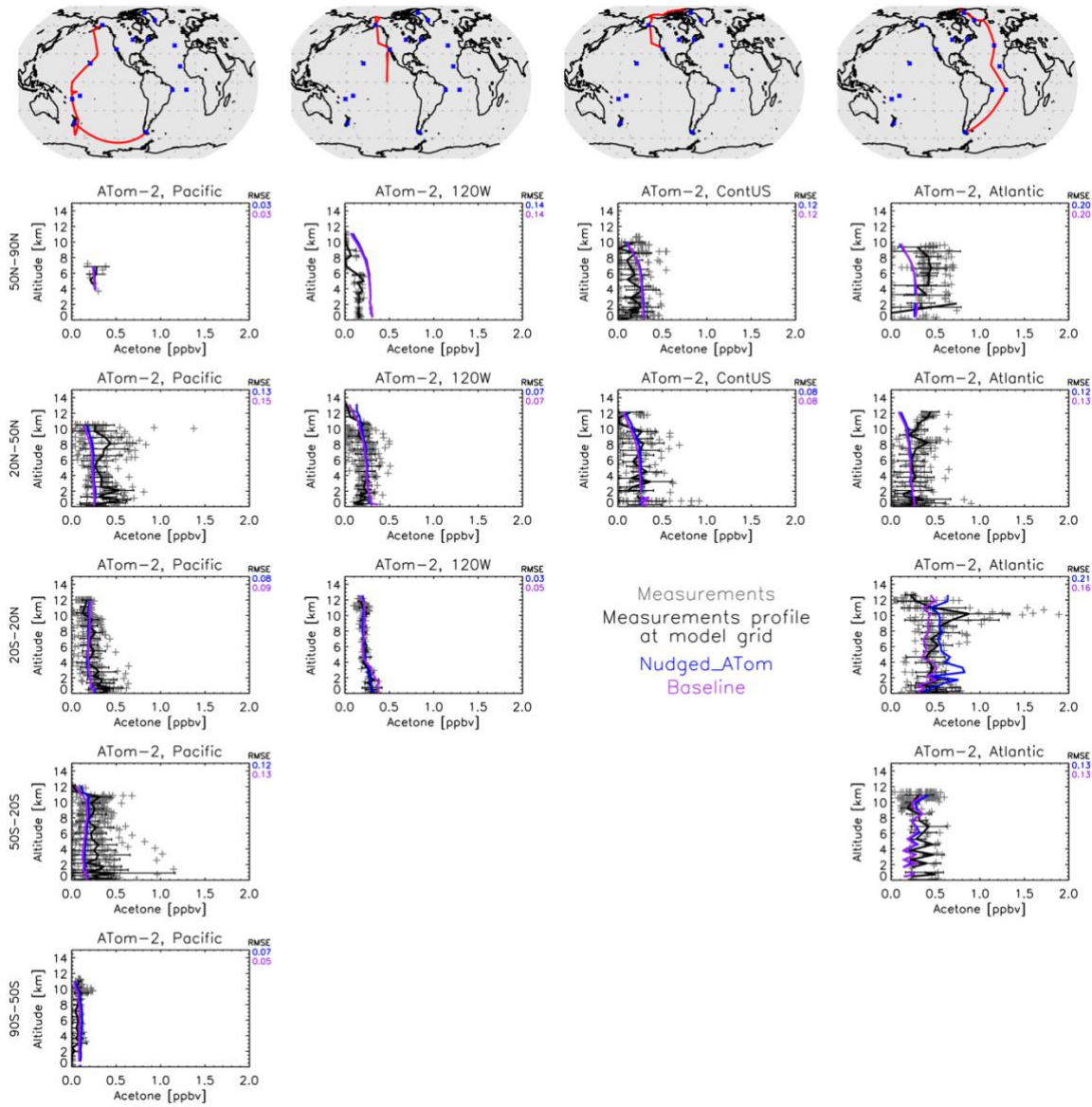


309

310 **Figure 7.** Baseline simulation acetone mixing ratios in the atmosphere at approximately 0-2 km (bottom), 2-6 km (middle), and 6-
 311 10 km (top) for the months of May-October (left) and November-April (right). The average mixing ratios over these broad altitude
 312 layers are weighted by the air mass in the model layers they contain. The choice of the slices and colors match those in Figure 1
 313 by (Fischer et al., 2012).

314

315 Additionally, the GISS ModelE2.1 was compared to four ATom campaigns (Thompson et al., 2022) of acetone field measurements
 316 in the atmosphere (Apel et al., 2021). For this comparison, we averaged the flight data to the model grid, and then compared the
 317 resulting mean against the monthly mean fields of the model output. Contrary to other chemical species measured during ATom
 318 that vary significantly in space and time, acetone has a rather long lifetime, and the data are collected for the most part very far
 319 from its sources. Combining that with the fact that prescribed emissions in the model vary by month, not by day or even hour in
 320 GISS ModelE2.1, makes such a comparison appropriate. Meteorology though can affect long-range transport significantly, so for
 321 that reason we performed a nudged simulation (called Nudged_ATOM) towards the MERRA-2 reanalysis (Gelaro et al., 2017), to
 322 capture such an effect more accurately. We also used emissions and greenhouse gas concentrations from the years of the ATom
 323 campaigns and varying with year, rather than the climatological means used in the Baseline simulation. Both the Nudged_ATOM
 324 and Baseline simulations are plotted in the ATom comparisons presented here (Figure 8).



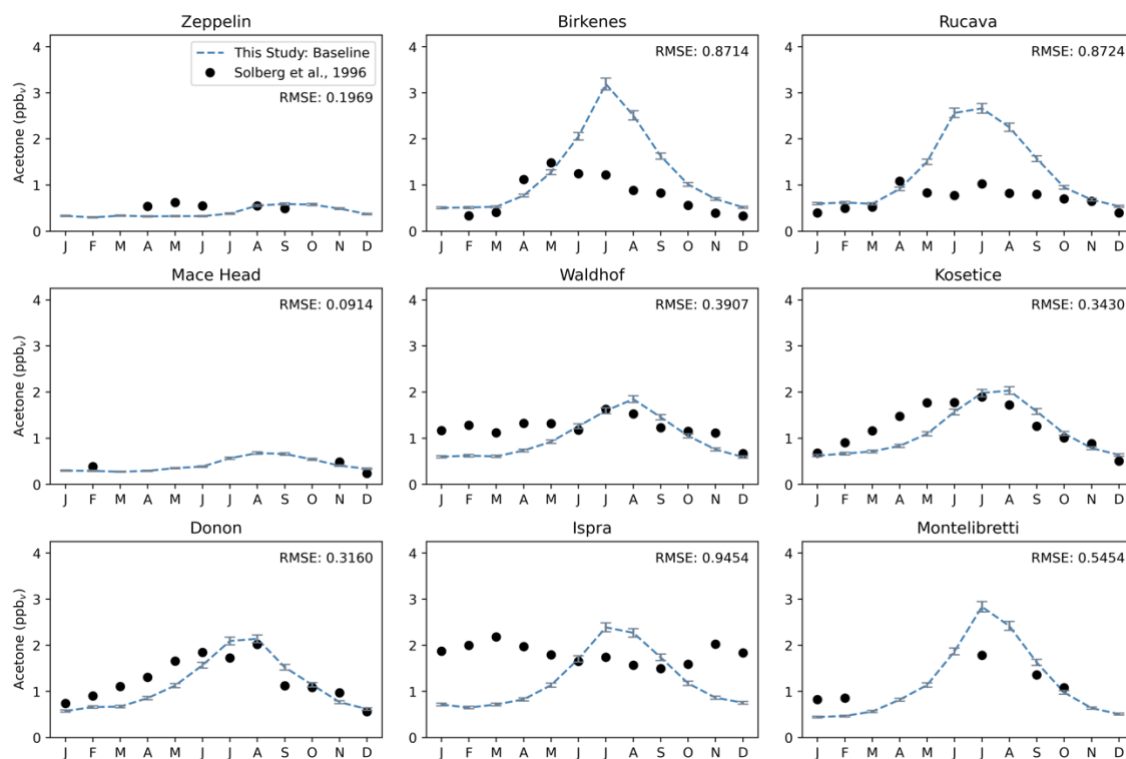
325
 326 **Figure 8.** Comparison between the GISS ModelE2.1 simulations (Baseline in purple and Nudged_ATOM in blue) and the ATom-
 327 2 field measurements (January-February 2017). Individual data points are shown with dark grey symbols, and their average values
 328 are shown in black, with error bars representing the one-sigma range of the averages. The root mean square error (RMSE) of each
 329 simulation is noted at the top right of each subplot.

330
 331 There are very few notable differences between the nudged and climatological simulations. An example is the tropical Atlantic
 332 Ocean, where during ATom-2 (Figure 8), the nudged simulation calculates higher acetone concentrations, but without gain of skill.
 333 Both model simulations miss the upper tropospheric peak that is found in the measurements, likely indicating a missing long-range
 334 transported plume. There is a similar result for ATom-3 (Figure S4) for the southern Atlantic Ocean mid-latitudes, where the
 335 nudged simulation is higher. Contrary to the ATom-2 case, both simulations for the ATom-3 case calculate an upper tropospheric
 336 maximum which is not found in the measurements. The tropical and southern mid-latitude Atlantic Ocean regions are both
 337 downwind of African biomass burning zones during ATom-2 and ATom-3, respectively, hinting to a primary and/or secondary
 338 incorrect source of acetone related with biomass burning and subsequent long-range transport. Other than those few cases, for the
 339 most part the two simulations are indistinguishable, indicating that our conclusions comparing climatological simulations to ATom

340 should be robust. (Figure 8, Figures S3-S5). This is important to remember in Section 3.5.3, where we perform sensitivity analyses
341 using climatological simulations and comparing against all four ATom campaigns.

342 3.4 Seasonality of acetone

343 Most European sites presented in Figure 3 have monthly-resolved measurements that can be used to analyze the seasonal behavior
344 of acetone in the model (Figure 9, Figure S6) (Solberg et al., 1996). These sites differ with respect to their geographic locations
345 and their proximity to anthropogenic sources. Zeppelin, Birkenes, Rucava, and Mace Head are all coastal sites, while Waldhof,
346 Kosetice, Donon, Ispra, and Montelibretti are inland sites. Regarding anthropogenic sources, Zeppelin is the most remote location
347 and Birkenes and Rucava each have small sources. Mace Head is a site affected by the marine boundary layer, and Waldhof,
348 Kosetice and Donon are sites with small local anthropogenic sources that are generally located in higher emission regions.
349 Montelibretti and particularly Ispra are subject to the highest anthropogenic sources. The measurements taken at Ispra show an
350 opposite seasonality than what is expected, and previous studies have considered this anomalous (Jacob et al., 2002).



351
352 **Figure 9.** Acetone over twelve months at nine European sites, similar to that of Jacob et al. (2002). The modeled estimates of
353 acetone at the surface from the Baseline simulation are shown as dashed blue lines and the grey error bars represent the one-sigma
354 range of the modeled concentrations in the climatological mean of 5 years. Field measurements from Solberg et al. (1996) are
355 shown as solid black dots. Root mean squared error between the Baseline simulation and field measurements are shown at the top
356 right of each subplot.

357
358 The GISS ModelE2.1 matches the seasonality of the measurements especially well in Zeppelin, Mace Head, Waldhof, Kosetice,
359 and Donon; the average root mean square error between the Baseline model and the measurements at these five sites are 0.27. The
360 Baseline model overestimates the measurements in Birkenes and Rucava ($RMSE = 0.87$ for both), even though these two sites
361 have low anthropogenic sources. This overestimation has been attributed to the vegetation source, which has a distinct seasonality

362 and is much stronger than any other source there. Interestingly, in Montelibretti, the model's overestimation of vegetation, yet
363 underestimation of local emissions, results in a decent estimation of the sources there (RMSE = 0.55) (Figure 9).

364

365 As mentioned previously, an analysis of the distribution of the regional sources and sinks at the nine European sites shows that,
366 except for Zeppelin and Mace Head, all studied European sites have vegetation as the dominant source that strongly contributes to
367 the simulated seasonality of concentrations (Figure S7). Vegetation sources peak in the summer months and are lower in the winter.
368 Deposition is a major sink of acetone that is comparable in magnitude with the vegetation source. Ocean uptake of acetone follows
369 a weak seasonal cycle, being stronger in the summer months. Relatively, the other fluxes (anthropogenic emissions, biomass
370 burning and ocean production) do not exhibit much seasonality at these locations (Figure S7).

371

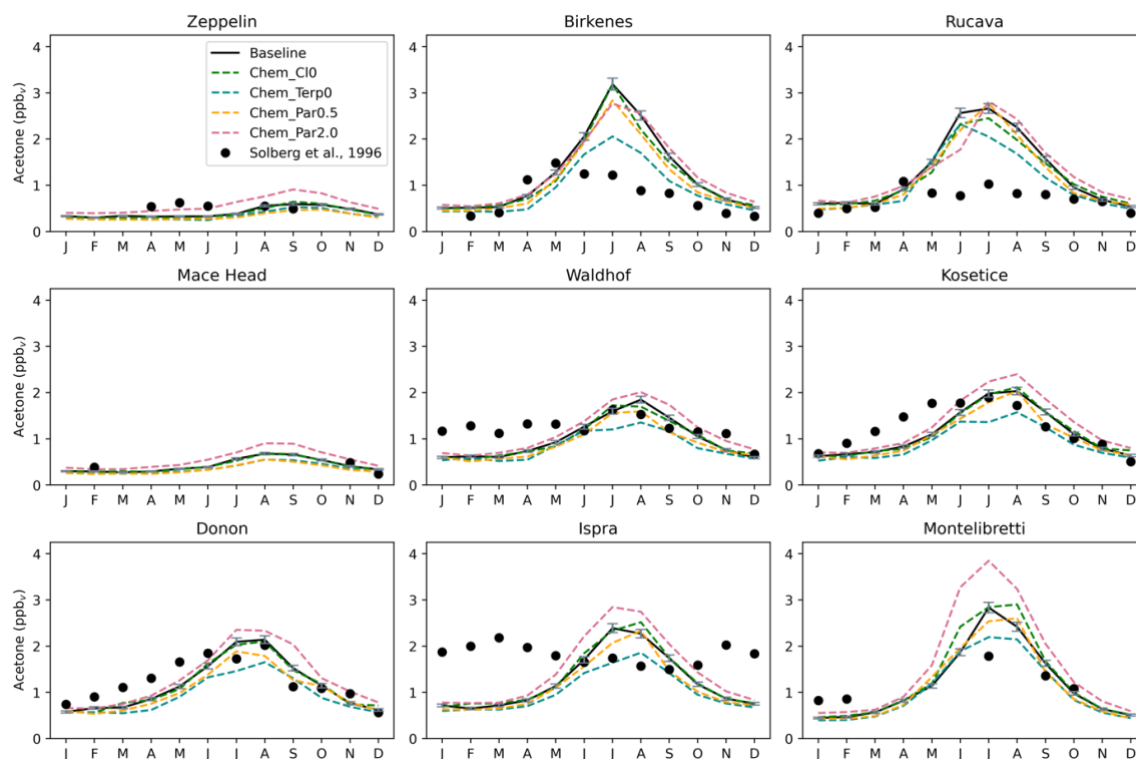
372 We also compared the GISS ModelE2.1's surface acetone at observation sites with less temporal coverage (Figure S8). In general,
373 the GISS ModelE2.1 matches the field measurements well. This is especially true for the non-summer seasons in Rosemount and
374 Berkeley, USA, and the summer peaks in Utrecht, Netherlands and Mainz, Germany. The model seems to be overestimating
375 acetone around Australia, as shown by comparisons with Cape Grim and Wollongong, while underestimating emissions in large
376 cities like Shenzhen and Beijing, China, London, UK, and Paris, France (Figure S8).

377 **3.5 Sensitivity studies**

378 The sensitivity simulations presented here have been described in Section 2.5 and in Table 1. We grouped them in two categories:
379 those directly related with chemical sources and sinks, and those related with terrestrial and oceanic acetone fluxes. Overall, the
380 sensitivity studies that presented the largest changes to total atmospheric burden included Chem_Terp0, Chem_Par0.5,
381 Chem_Par2.0, Veg_0.7, Ocn_2.0, and Dep_f0 (all but Chem_Cl0 and BB_2.0) (Figures S9-S14).

382 **3.5.1 Chemistry**

383 Chemistry sensitivity tests that modified the production of acetone were analyzed with respect to the budget and global distribution
384 of acetone. In the Chem_Cl0 simulation, where no acetone oxidation by the chlorine radical occurs, the overall global acetone
385 budget does not change. However, in some places like Rucava, Ispra, Montelibretti, and Shenzhen, the shape of the acetone
386 concentration profile over the year changes slightly (Figure 10, Figure S15).



387

388

389

390

391

392

393

394

395

396

397

398

399

400

401

402

403

404

405

406

407

408

409

410

Figure 10. Similar to Figure 9, but with the chemistry sensitivity studies added. The modeled estimates of acetone at the surface from the Baseline simulation are shown as solid black lines, and the sensitivity studies are as follows: removing the acetone + chlorine reaction (dashed green lines), removing the production of acetone from terpenes (dashed blue lines), halving the yield of acetone from paraffin (dashed orange lines), and doubling the yield of acetone from paraffin (dashed pink lines). Field measurements from Solberg et al., (1996) are shown as solid black dots.

The Chem_Terp0 simulation that removes the production of acetone from terpenes decreases the summer peak of acetone by as much as 35.5% in Birkenes, 25.5% in Mainz, and 25.3% in Berkeley (Figure 10, Figure S15). Other sites like Montelibretti, Ispra and Paris have their summer peak decreased by 22.6%, 22.2%, and 19.0%, respectively (Figure 10, Figure S15). Coastal and remote areas like Zeppelin, Mace Head and Dumont d’Urville, Antarctica are not impacted by the removal of terpenes (Figure 10, Figure S15).

There seems to be some nonlinearities with the relationship between acetone abundance and its yield from paraffin, as the results from the Chem_Par2.0 and Chem_Par0.5 simulation reveal that doubling the yield has a stronger impact than halving it. For instance, in Montelibretti, doubling the yield from paraffin increases the summer peak by 35.7%, while halving the yield decreases the summer peak by only 8.3% (Figure 10). A similar relationship is observed at other sites: Ispra (19.1% increase with double paraffin, 2.5% decrease with half paraffin) and Berkeley (12.7% increase with double paraffin, 2.5% decrease with half paraffin) (Figure 10, Figure S15). Overall, we explored chemistry sensitivities that would tend to push acetone in both directions. The Baseline simulation falls between our tests, which we have identified as important uncertainties.

The spatial distribution differences between the chemistry sensitivity studies and the Baseline simulation show some interesting patterns (Figure S16). Removing the production of acetone from terpenes oxidation in the Chem_Terp0 simulation decreased acetone over the continents, and especially over tropical and boreal forests which are where terpenes are emitted. This change also

411 increased acetone concentrations over the oceans due to chemical composition changes downwind that result from the change of
412 terpenes oxidation products (Figure S16, top left). Halving production of acetone from paraffin oxidation in the Chem_Par0.5
413 simulation only decreased acetone concentrations over the continents, while doubling it in the Chem_Par2.0 simulation increased
414 acetone concentrations over the continents and strengthened acetone destruction over the tropical oceans (Figure S16, top right and
415 bottom middle, respectively). Setting the acetone + chlorine reaction rate to 0 in the Chem_Cl0 simulation resulted in negligible
416 changes across the globe (anomalies of $<0.4 \text{ ng m}^{-2} \text{ s}^{-1}$).

417 **3.5.2 Terrestrial and oceanic fluxes**

418 Terrestrial and oceanic fluxes sensitivities were analyzed at the same sites. The vegetation flux sensitivity, Veg_0.7, reduced
419 acetone production from MEGAN by 30%. This change decreased the summer peak of acetone down at nearly every location
420 studied, but most notably by 32.6% in Birkenes, 22.9% in Rucava, and 22.2% in Rosemount (Figures S17, S18).

421
422 In the oceanic flux sensitivity simulation, Ocn_2.0, the concentration of acetone in the water was doubled from 15 nM to 30 nM.
423 The results of this simulation varied with geographic location. For instance, in Birkenes, doubling ocean concentration reduced
424 overall acetone by 13.9%, while in Montelibretti, it was increased by 16.1% (Figure S17). Even though Birkenes is more of a
425 coastal city than Montelibretti, this result may simply be a temperature effect; Birkenes is at 58°N , while Montelibretti is at
426 42°N , and a warmer ocean may produce more acetone. Overall, in most places, the doubling ocean acetone concentration did not
427 change much atmospheric acetone throughout the year (Figures S17, S18).

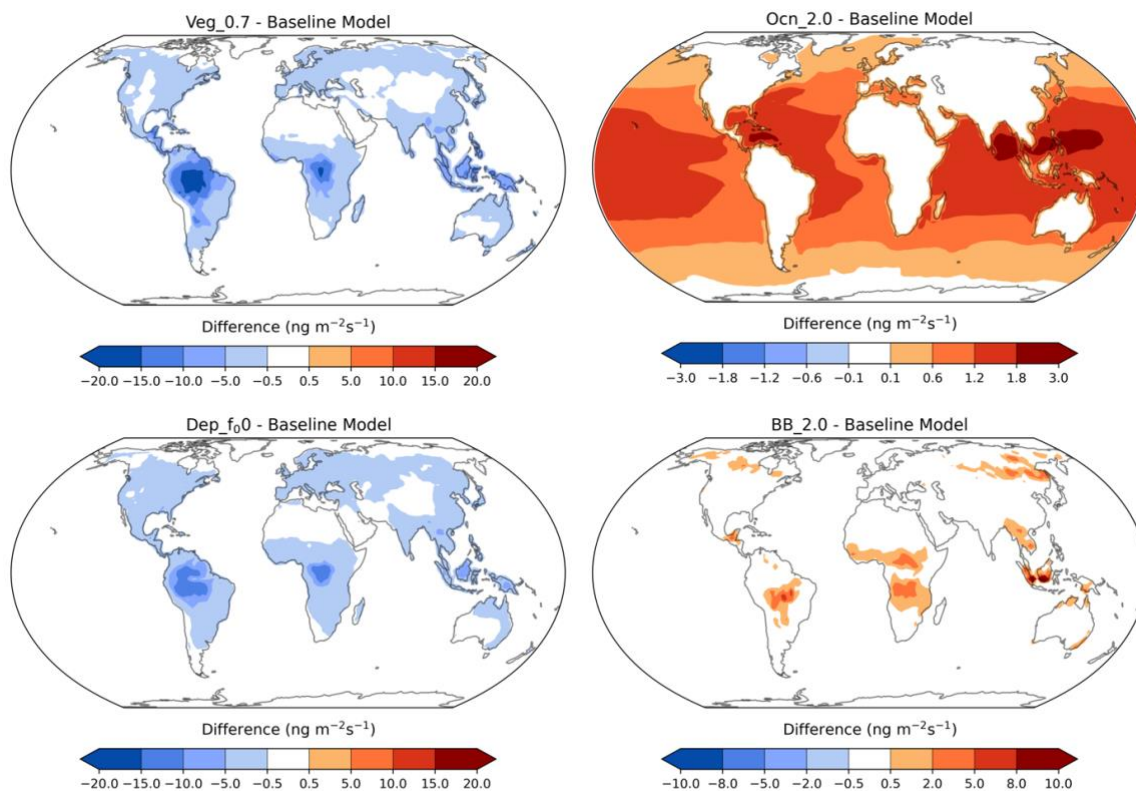
428
429 Another broader finding from the ocean sensitivity study is that doubling the ocean acetone concentration impacted oceanic
430 emissions of acetone more than the oceanic uptake of acetone (Figure S13). Specifically, in this sensitivity study the emissions
431 doubled while the uptake only increased by 40%. This difference may be attributed to the fact that a higher ocean concentration
432 will generally cause less resistance in the emission direction, but more resistance in the uptake direction. The differences in
433 oceanic acetone emissions and uptakes in this sensitivity study also resulted in increased chemical destruction, and an overall
434 higher burden of acetone in the atmosphere (Figure S13).

435
436 In the dry deposition sensitivity simulation, the reactivity factor, f_0 , was reduced from 0.1 to 0. As a result, the amount of acetone
437 removed by deposition decreased, and the atmospheric acetone concentration increased. The strongest increases were found to be
438 in Ispra (38.4%), Kosetice (37.9%), Paris (37.9%), Beijing (37.3%), Donon (36.6%), Mainz (33.4%), Montelibretti (30.5%),
439 Rosemount (28.9%), Berkeley (28.7%), and Waldhof (28.7%) (Figures S17, S18).

440
441 The final terrestrial fluxes sensitivity study, BB_2.0, doubled biomass burning emissions. This sensitivity did not significantly
442 change acetone mixing ratios in any of the locations studied, except an increased summer spike (12.7%) in Birkenes (Figure S17).
443 Most of the locations studied were far from biomass burning sites to begin with, however, so an analysis of this sensitivity study
444 over biomass burning hotspots is needed.

445
446 The acetone concentration anomalies around the world between the terrestrial and oceanic fluxes sensitivity studies and the
447 Baseline simulation are presented in Figure 11. Decreasing acetone production from MEGAN vegetation by 30% resulted in a
448 decrease of acetone mixing ratios over the tropical and boreal forests, where this source is most prominent (Figure 11, top left).
449 Doubling ocean acetone concentrations increased production of acetone from the oceans globally. This increase was stronger in

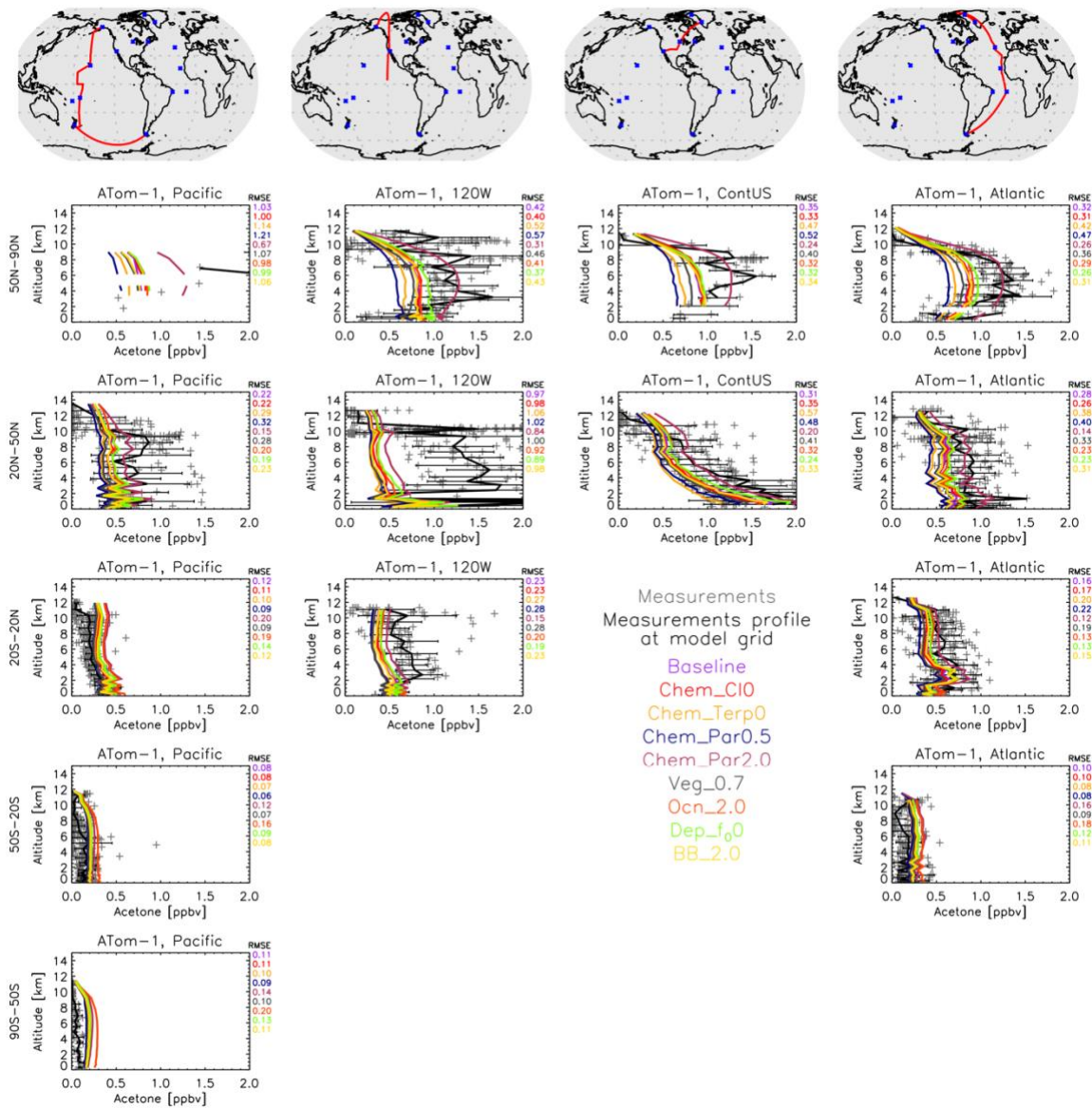
450 the tropics, due to the higher sea surface temperatures (Figure 11, top right). Reducing the reactivity factor for dry deposition
 451 decreased the amount of acetone removed by deposition over the continents (Figure 11, bottom left), in particular where acetone
 452 concentration is elevated (Figure 3). Finally, doubling biomass burning emissions did not change acetone mixing ratios much,
 453 other than over biomass burning hotspots like central South America, central Africa, Southeast Asia, and Siberia (Figure 11, bottom
 454 right).



455
 456 **Figure 11.** Acetone anomalies from the Baseline simulation for the vegetation (top left), ocean (top right), dry deposition (bottom
 457 left) and biomass burning (bottom right) sensitivities, with red indicating an increase and blue indicating a decrease of the specific
 458 flux. Nonlinear colorbars are used to better differentiate the details in the map.

459 3.5.3 ATom comparisons

460 The ATom comparisons were replicated with the sensitivity simulations (Figure 12, Figures S19-S21). Doubling the paraffin
 461 yield of acetone seemed to have the most noticeable impacts on the vertical profiles. As seen during ATom-1 (July-August
 462 2016), doubling the paraffin yield decreases the root mean square error (RMSE) against measurements in the Northern
 463 hemisphere polar atmosphere and brings the model to closer agreement to observations, but decreases the agreement throughout
 464 the remote Pacific Ocean, which implies different chemical formation pathways over the more polluted northern hemisphere on
 465 the Atlantic Ocean side, compared to the Pacific Ocean. Nearly the exact opposite is calculated in the case of the halving of the
 466 paraffin yield of acetone, which adds confidence to the chemical pathway explanation (Figure 12). The doubling of the ocean
 467 acetone concentration shows a small improvement (decrease) in the RMSE over the tropical and north Atlantic Ocean during
 468 ATom-1 and an even smaller decrease over the north hemisphere Pacific Ocean, but an increase over the tropical and south
 469 Pacific Ocean, showing the potential role of different ocean concentrations of acetone across the globe (Figure 12). It needs to be
 470 noted though that the model performs fairly well in those regions already, so the small improvements mentioned do not largely
 471 affect the regional acetone concentrations, as also expected due to the rather weak acetone source from the ocean.



472
 473 **Figure 12.** Similar to Figure 8, except a comparison between the GISS ModelE2.1 sensitivity simulations and the ATom-1 aircraft
 474 measurements (July-August 2016). Individual data points are shown with dark grey symbols, and their average values are shown
 475 in black, with error bars representing the one-sigma range of the averages. The root mean square error (RMSE) of each simulation
 476 is notes at the top right of each subplot. Note that all sensitivities are to be compared against the Baseline simulation, not the
 477 Nudged_ATOM one, but as shown earlier this makes very little difference in the comparison with observations (Figure 8).

478
 479 The simulations of the boreal winter (January-February 2017) score the best against ATom-2 (Figure S19). Acetone
 480 concentrations are the lowest during that period in both hemispheres, a direct result from the very low biomass burning
 481 emissions, which is among the highest acetone sources worldwide. In the region north of 50N, the increase of both the paraffin
 482 source and the oceanic source of acetone degrade the simulations, and the same applies for the observations around 102W
 483 longitude, especially at mid-latitudes. The increase in oceanic source over the northern hemisphere mid-latitude Pacific Ocean
 484 improves (decreases) RMSE, but as already mentioned, the low concentrations of acetone in that area (and in general during
 485 ATom-2) show that there is small sensitivity in the modified acetone sources to acetone profiles. While the ocean flux may be

486 small, these ATom comparisons reveal that they especially matter in the southern latitudes. These are the same latitudes where
487 the ocean appears to be in equilibrium (neither a strong source nor sink) (Figure 5).

488
489 During boreal fall (ATom-3), doubling the paraffin yield tends to overshoot most of the observations (Figure S20), contrary to
490 what was calculated during boreal summer (ATom-1; Figure 12). This is the case for most ATom-3 Atlantic Ocean flights, while
491 an improvement is calculated when comparing with the flights near the west coast of the US or the Pacific Ocean mid-latitudes.
492 These results reveal that the model may be underestimating a paraffin source during boreal summer, which diminishes during
493 boreal fall.

494
495 The boreal spring season (April-May 2018; ATom-4; Figure S21) is the hardest for the model to simulate when it comes to
496 northern hemisphere concentrations. All sensitivity studies greatly underestimate observations, in particular the long-range
497 transport upper tropospheric amount near the polar latitudes but also the concentrations measured throughout the troposphere at
498 northern mid-latitudes. The model skillfully simulates tropical and southern hemisphere profiles, while it cannot reproduce the
499 higher concentrations at northern latitudes. The increased yield from paraffin or the increased oceanic concentration do reduce
500 RMSE, but still fall short on capturing the magnitude, or the shape, of the profiles of the spring hemisphere. We cannot infer
501 from our model simulations whether this is a missing source or an overestimated sink, but the latter appears to be more plausible,
502 given the large underestimation of all modeled profiles at northern mid-latitudes. In the southern hemisphere, the increase of
503 oceanic acetone clearly degrades model skill, as was frequently the case during the other campaigns presented above.
504 It is worth mentioning that for most cases the changes in the source of acetone do not alter the shape of the vertical profile. This
505 means that the transport or chemical sinks of acetone dictate its spatiotemporal distribution more than sources, while the sources
506 do affect the magnitude of that distribution, quite significantly under some of the sensitivity simulations described here.

507 **4 Conclusion**

508 The development of acetone's representation in the NASA GISS ModelE2.1 from its previous simplistic parameterization of
509 instantaneous isoprene to a full tracer experiencing transport, chemistry, emissions, and deposition of its own, marks a significant
510 improvement to the model's chemical scheme. Calculations of the 3-dimensional distribution of acetone as a function of time, as
511 well as evaluations of its atmospheric burden and source/sink fluxes demonstrate the complexity of acetone's spatiotemporal
512 distribution in the atmosphere. An analysis was conducted to assess the simulated global acetone budget in the context of past
513 modeling studies. Further comparisons were made against field observations on a variety of spatial and temporal scales, which
514 indicated that the model agrees well with surface field measurements and vertical profiles in the remote atmosphere. The chemical
515 formation of acetone from precursor compounds such as paraffin was found to be an uncertain yet impactful factor. Vegetation
516 fluxes as calculated by MEGAN were identified as the dominant acetone source which dictates its seasonality. Additionally, the
517 acetone concentration in seawater was found to affect oceanic sources more than oceanic sinks.

518
519 Any feedback between acetone and the rest of the chemistry, and particularly ozone, have not been assessed here, and should be
520 the goal of a future study. Additionally, the current ocean-acetone interaction uses a constant concentration of acetone in the ocean.
521 It will be helpful to test a more realistic, non-uniform ocean acetone concentration, when this becomes available. Finally, other
522 atmospheric conditions such as surface wind speed may be considered further when modifying the ocean scheme.

523 **Code Availability**

524 The GISS ModelE code is publicly available at <https://simplex.giss.nasa.gov/snapshots/>. The most recent public version is E.2.1.2;
525 the version of the code used here is already committed in the non-public-facing repository and will be released in the future
526 following the regular release cycle of ModelE, under version E3.1.

527 **Data Availability**

528 We have made available the simulated three-dimensional distributions of acetone from each simulation described in the paper
529 (Baseline, sensitivity simulations in Table 1, and Nudged_ATOM). These are found in zip files, grouped by simulation, here:
530 <https://doi.org/10.5281/zenodo.7567614>. Each zip file contains a series of netCDF format files with filenames
531 {month}_5yrAvg_Acetone_{simulation}.nc, where each file is a climatological average over 5 years of repeated forcing
532 conditions.

533
534 The exception is the transient-forcing simulation "Nudged_ATOM", which contains single-month averages of acetone from JUL
535 2016 through MAY 2018, to cover the ATom observational period. The file names for that simulation are of the form:
536 {month}_{year}_Acetone_Nudged_ATOM.nc. Acetone is in ppb_v units and given on the model's native grid and vertical levels.
537 These are hybrid sigma levels, but nominal pressure middles and edges are given in the plm and ple variables, respectively, and
538 the grid box surface areas are also provided.

539 **Author Contribution**

540 KT conceived the study and guided the model development which was done by GF. All simulations presented here were performed
541 by GF. DS advised during the whole development process. AR did the literature search and all comparisons against other modeling
542 studies. With the exception of the ATom analysis and plots which were done by KT, and comparisons against field measurements
543 and the rest of the plots were done by AR. AR drafted the first version of the manuscript, and all authors contributed to it. GF
544 prepared all model outputs for dissemination.

545 **Competing Interests**

546 The authors declare that they have no conflict of interest.

547 **Acknowledgements**

548 Climate modeling at GISS is supported by the NASA Modeling, Analysis and Prediction program. AR acknowledges support from
549 North Carolina Space Grant and the NASA Office of STEM Engagement. Resources supporting this work were provided by the
550 NASA High-End Computing (HEC) Program through the NASA Center for Climate Simulation (NCCS) at Goddard Space Flight
551 Center.

552 **References**

553 Apel, E. C., Asher, E. C., Hills, A. J., and Hornbrook, R. S.: ATom: Volatile Organic Compounds (VOCs) from the TOGA
554 instrument, Version 2, ORNL DAAC, <https://doi.org/10.3334/ORNLDAAC/1936>, 2021.

555 Arnold, S. R., Chipperfield, M. P., and Blitz, M. A.: A three-dimensional model study of the effect of new temperature-dependent
556 quantum yields for acetone photolysis, *J. Geophys. Res. Atmospheres*, 110, <https://doi.org/10.1029/2005JD005998>, 2005.

557 Beale, R., Dixon, J. L., Arnold, S. R., Liss, P. S., and Nightingale, P. D.: Methanol, acetaldehyde, and acetone in the surface waters
558 of the Atlantic Ocean, *J. Geophys. Res. Oceans*, 118, 5412–5425, <https://doi.org/10.1002/jgrc.20322>, 2013.

559 Benkelberg, H.-J., Hamm, S., and Warneck, P.: Henry’s law coefficients for aqueous solutions of acetone, acetaldehyde and
560 acetonitrile, and equilibrium constants for the addition compounds of acetone and acetaldehyde with bisulfite, *J. Atmospheric*
561 *Chem.*, 20, 17–34, <https://doi.org/10.1007/BF01099916>, 1995.

562 Brewer, J. F., Bishop, M., Kelp, M., Keller, C. A., Ravishankara, A. R., and Fischer, E. V.: A sensitivity analysis of key natural
563 factors in the modeled global acetone budget, *J. Geophys. Res. Atmospheres*, 122, 2043–2058,
564 <https://doi.org/10.1002/2016JD025935>, 2017.

565 Chin, M., Jacob, D. J., Gardner, G. M., Foreman-Fowler, M. S., Spiro, P. A., and Savoie, D. L.: A global three-dimensional model
566 of tropospheric sulfate, *J. Geophys. Res. Atmospheres*, 101, 18667–18690, <https://doi.org/10.1029/96JD01221>, 1996.

567 Dolgorouky, C., Gros, V., Sarda-Estève, R., Sinha, V., Williams, J., Marchand, N., Sauvage, S., Poulain, L., Sciare, J., and
568 Bonsang, B.: Total OH reactivity measurements in Paris during the 2010 MEGAPOLI winter campaign, *Atmospheric Chem. Phys.*,
569 12, 9593–9612, <https://doi.org/10.5194/acp-12-9593-2012>, 2012.

570 Dufour, G., Szopa, S., Harrison, J. J., Boone, C. D., and Bernath, P. F.: Seasonal variations of acetone in the upper troposphere–
571 lower stratosphere of the northern midlatitudes as observed by ACE-FTS, *J. Mol. Spectrosc.*, 323, 67–77,
572 <https://doi.org/10.1016/j.jms.2016.02.006>, 2016.

573 Elias, T., Szopa, S., Zahn, A., Schuck, T., Brenninkmeijer, C., Sprung, D., and Slemr, F.: Acetone variability in the upper
574 troposphere: analysis of CARIBIC observations and LMDz-INCA chemistry-climate model simulations, *Atmospheric Chem.*
575 *Phys.*, 11, 8053–8074, <https://doi.org/10.5194/acp-11-8053-2011>, 2011.

576 Fischbeck, G., Bönisch, H., Neumaier, M., Brenninkmeijer, C. A. M., Orphal, J., Brito, J., Becker, J., Sprung, D., van Velthoven,
577 P. F. J., and Zahn, A.: Acetone–CO enhancement ratios in the upper troposphere based on 7 years of CARIBIC data: new insights
578 and estimates of regional acetone fluxes, *Atmospheric Chem. Phys.*, 17, 1985–2008, <https://doi.org/10.5194/acp-17-1985-2017>,
579 2017.

580 Fischer, E. V., Jacob, D. J., Millet, D. B., Yantosca, R. M., and Mao, J.: The role of the ocean in the global atmospheric budget of
581 acetone, *Geophys. Res. Lett.*, 39, <https://doi.org/10.1029/2011GL050086>, 2012.

582 Folberth, G. A., Hauglustaine, D. A., Lathière, J., and Brocheton, F.: Interactive chemistry in the Laboratoire de Météorologie
583 Dynamique general circulation model: model description and impact analysis of biogenic hydrocarbons on tropospheric chemistry,
584 *Atmospheric Chem. Phys.*, 6, 2273–2319, <https://doi.org/10.5194/acp-6-2273-2006>, 2006.

585 Fujimori, S., Hasegawa, T., Masui, T., Takahashi, K., Herran, D. S., Dai, H., Hijioka, Y., and Kainuma, M.: SSP3: AIM
586 implementation of Shared Socioeconomic Pathways, *Glob. Environ. Change*, 42, 268–283,
587 <https://doi.org/10.1016/j.gloenvcha.2016.06.009>, 2017.

588 Galbally, I., Lawson, S. J., Bentley, S., Gillett, R., Meyer, M., and Goldstein, A.: Volatile organic compounds in marine air at Cape
589 Grim, Australia, *Environ. Chem. - Env. CHEM*, 4, <https://doi.org/10.1071/EN07024>, 2007.

590 Gelaro, R., McCarty, W., Suárez, M. J., Todling, R., Molod, A., Takacs, L., Randles, C. A., Darmenov, A., Bosilovich, M. G.,
591 Reichle, R., Wargan, K., Coy, L., Cullather, R., Draper, C., Akella, S., Buchard, V., Conaty, A., Silva, A. M. da, Gu, W., Kim, G.-
592 K., Koster, R., Lucchesi, R., Merkova, D., Nielsen, J. E., Partyka, G., Pawson, S., Putman, W., Rienecker, M., Schubert, S. D.,
593 Sienkiewicz, M., and Zhao, B.: The Modern-Era Retrospective Analysis for Research and Applications, Version 2 (MERRA-2),
594 *J. Clim.*, 30, 5419–5454, <https://doi.org/10.1175/JCLI-D-16-0758.1>, 2017.

595 de Gouw, J., Warneke, C., Holzinger, R., Klüpfel, T., and Williams, J.: Inter-comparison between airborne measurements of
596 methanol, acetonitrile and acetone using two differently configured PTR-MS instruments, *Int. J. Mass Spectrom.*, 239, 129–137,
597 <https://doi.org/10.1016/j.ijms.2004.07.025>, 2004.

598 Guenther, A. B., Jiang, X., Heald, C. L., Sakulyanontvittaya, T., Duhl, T., Emmons, L. K., and Wang, X.: The Model of Emissions of
599 of Gases and Aerosols from Nature version 2.1 (MEGAN2.1): an extended and updated framework for modeling biogenic
600 emissions, *Geosci. Model Dev.*, 5, 1471–1492, <https://doi.org/10.5194/gmd-5-1471-2012>, 2012.

601 Guérette, É.-A., Paton-Walsh, C., Galbally, I., Molloy, S., Lawson, S., Kubistin, D., Buchholz, R., Griffith, D. W. T., Langenfelds,
602 R. L., Krummel, P. B., Loh, Z., Chambers, S., Griffiths, A., Keywood, M., Selleck, P., Dominick, D., Humphries, R., and Wilson,
603 S. R.: Composition of Clean Marine Air and Biogenic Influences on VOCs during the MUMBA Campaign, *Atmosphere*, 10, 383,
604 <https://doi.org/10.3390/atmos10070383>, 2019.

605 Hoesly, R. M., Smith, S. J., Feng, L., Klimont, Z., Janssens-Maenhout, G., Pitkanen, T., Seibert, J. J., Vu, L., Andres, R. J., Bolt,
606 R. M., Bond, T. C., Dawidowski, L., Kholod, N., Kurokawa, J., Li, M., Liu, L., Lu, Z., Moura, M. C. P., O'Rourke, P. R., and
607 Zhang, Q.: Historical (1750–2014) anthropogenic emissions of reactive gases and aerosols from the Community Emissions Data
608 System (CEDS), *Geosci. Model Dev.*, 11, 369–408, <https://doi.org/10.5194/gmd-11-369-2018>, 2018.

609 Hu, L., Millet, D. B., Kim, S. Y., Wells, K. C., Griffis, T. J., Fischer, E. V., Helmig, D., Hueber, J., and Curtis, A. J.: North
610 American acetone sources determined from tall tower measurements and inverse modeling, *Atmospheric Chem. Phys.*, 13, 3379–
611 3392, <https://doi.org/10.5194/acp-13-3379-2013>, 2013.

612 Huang, X.-F., Zhang, B., Xia, S.-Y., Han, Y., Wang, C., Yu, G.-H., and Feng, N.: Sources of oxygenated volatile organic
613 compounds (OVOCs) in urban atmospheres in North and South China, *Environ. Pollut.*, 261, 114152,
614 <https://doi.org/10.1016/j.envpol.2020.114152>, 2020.

615 Jacob, D. J., Field, B. D., Jin, E. M., Bey, I., Li, Q., Logan, J. A., Yantosca, R. M., and Singh, H. B.: Atmospheric budget of
616 acetone, *J. Geophys. Res. Atmospheres*, 107, ACH 5-1-ACH 5-17, <https://doi.org/10.1029/2001JD000694>, 2002.

617 Johnson, M. T.: A numerical scheme to calculate temperature and salinity dependent air-water transfer velocities for any gas,
618 *Ocean Sci.*, 6, 913–932, <https://doi.org/10.5194/os-6-913-2010>, 2010.

619 Kelley, M., Schmidt, G. A., Nazarenko, L. S., Bauer, S. E., Ruedy, R., Russell, G. L., Ackerman, A. S., Aleinov, I., Bauer, M.,
620 Bleck, R., Canuto, V., Cesana, G., Cheng, Y., Clune, T. L., Cook, B. I., Cruz, C. A., Genio, A. D. D., Elsaesser, G. S., Faluvegi,
621 G., Kiang, N. Y., Kim, D., Lacis, A. A., Leboissetier, A., LeGrande, A. N., Lo, K. K., Marshall, J., Matthews, E. E., McDermid,
622 S., Mezuman, K., Miller, R. L., Murray, L. T., Oinas, V., Orbe, C., García-Pando, C. P., Perlwitz, J. P., Puma, M. J., Rind, D.,
623 Romanou, A., Shindell, D. T., Sun, S., Tausnev, N., Tsigaridis, K., Tselioudis, G., Weng, E., Wu, J., and Yao, M.-S.: GISS-E2.1:
624 Configurations and Climatology, *J. Adv. Model. Earth Syst.*, 12, e2019MS002025, <https://doi.org/10.1029/2019MS002025>, 2020.

625 Khan, M. A. H., Cooke, M. C., Utembe, S. R., Archibald, A. T., Maxwell, P., Morris, W. C., Xiao, P., Derwent, R. G., Jenkin, M.
626 E., Percival, C. J., Walsh, R. C., Young, T. D. S., Simmonds, P. G., Nickless, G., O'Doherty, S., and Shallcross, D. E.: A study of
627 global atmospheric budget and distribution of acetone using global atmospheric model STOCHEM-CRI, *Atmos. Environ.*, 112,
628 269–277, <https://doi.org/10.1016/j.atmosenv.2015.04.056>, 2015.

629 Koch, D., Jacob, D., Tegen, I., Rind, D., and Chin, M.: Tropospheric sulfur simulation and sulfate direct radiative forcing in the
630 Goddard Institute for Space Studies general circulation model, *J. Geophys. Res. Atmospheres*, 104, 23799–23822,
631 <https://doi.org/10.1029/1999JD900248>, 1999.

632 Langford, B., Nemitz, E., House, E., Phillips, G. J., Famulari, D., Davison, B., Hopkins, J. R., Lewis, A. C., and Hewitt, C. N.:
633 Fluxes and concentrations of volatile organic compounds above central London, UK, *Atmospheric Chem. Phys.*, 10, 627–645,
634 <https://doi.org/10.5194/acp-10-627-2010>, 2010.

635 Lewis, A. C., Hopkins, J. R., Carpenter, L. J., Stanton, J., Read, K. A., and Pilling, M. J.: Sources and sinks of acetone, methanol,
636 and acetaldehyde in North Atlantic marine air, *Atmospheric Chem. Phys.*, 5, 1963–1974, <https://doi.org/10.5194/acp-5-1963-2005>,
637 2005.

638 Li, K., Li, J., Tong, S., Wang, W., Huang, R.-J., and Ge, M.: Characteristics of wintertime VOCs in suburban and urban Beijing:
639 concentrations, emission ratios, and festival effects, *Atmospheric Chem. Phys.*, 19, 8021–8036, <https://doi.org/10.5194/acp-19-8021-2019>, 2019.

641 Liss, P. S. and Slater, P. G.: Flux of Gases across the Air-Sea Interface, *Nature*, 247, 181–184, <https://doi.org/10.1038/247181a0>,
642 1974.

643 Marandino, C. A., Bruyn, W. J. D., Miller, S. D., Prather, M. J., and Saltzman, E. S.: Oceanic uptake and the global atmospheric
644 acetone budget, *Geophys. Res. Lett.*, 32, <https://doi.org/10.1029/2005GL023285>, 2005.

645 van Marle, M. J. E., Kloster, S., Magi, B. I., Marlon, J. R., Daniau, A.-L., Field, R. D., Arneeth, A., Forrest, M., Hantson, S.,
646 Kehrwald, N. M., Knorr, W., Lasslop, G., Li, F., Mangeon, S., Yue, C., Kaiser, J. W., and van der Werf, G. R.: Historic global
647 biomass burning emissions for CMIP6 (BB4CMIP) based on merging satellite observations with proxies and fire models (1750–
648 2015), *Geosci. Model Dev.*, 10, 3329–3357, <https://doi.org/10.5194/gmd-10-3329-2017>, 2017.

649 Met Office, Hadley Centre: HadISST 1.1 - Global sea-Ice coverage and SST (1870-Present), [Internet]. NCAS British
650 Atmospheric Data Centre 2006, April 3, 2021. Available from
651 http://badc.nerc.ac.uk/view/badc.nerc.ac.uk__ATOM__dataent_hadisst, 2006.

652 Neu, J. L., Prather, M. J., and Penner, J. E.: Global atmospheric chemistry: Integrating over fractional cloud cover, *J. Geophys.*
653 *Res. Atmospheres*, 112, 2006JD008007, <https://doi.org/10.1029/2006JD008007>, 2007.

654 O'Rourke, P. R., Smith, S. J., Mott, A., Ahsan, H., McDuffie, E. E., Crippa, M., Klimont, Z., McDonald, B., Wang, S., Nicholson,
655 M. B., Feng, L., and Hoesly, R. M.: CEDS v_2021_04_21 Release Emission Data, <https://doi.org/10.5281/zenodo.4741285>, 2021.

656 Read, K. A., Carpenter, L. J., Arnold, S. R., Beale, R., Nightingale, P. D., Hopkins, J. R., Lewis, A. C., Lee, J. D., Mendes, L., and
657 Pickering, S. J.: Multiannual Observations of Acetone, Methanol, and Acetaldehyde in Remote Tropical Atlantic Air: Implications
658 for Atmospheric OVOC Budgets and Oxidative Capacity, *Environ. Sci. Technol.*, 46, 11028–11039,
659 <https://doi.org/10.1021/es302082p>, 2012.

660 Riahi, K., van Vuuren, D. P., Kriegler, E., Edmonds, J., O'Neill, B. C., Fujimori, S., Bauer, N., Calvin, K., Dellink, R., Fricko, O.,
661 Lutz, W., Popp, A., Cuaresma, J. C., Kc, S., Leimbach, M., Jiang, L., Kram, T., Rao, S., Emmerling, J., Ebi, K., Hasegawa, T.,
662 Havlik, P., Humpenöder, F., Da Silva, L. A., Smith, S., Stehfest, E., Bosetti, V., Eom, J., Gernaat, D., Masui, T., Rogelj, J., Strefler,
663 J., Drouet, L., Krey, V., Luderer, G., Harmsen, M., Takahashi, K., Baumstark, L., Doelman, J. C., Kainuma, M., Klimont, Z.,
664 Marangoni, G., Lotze-Campen, H., Obersteiner, M., Tabeau, A., and Tavoni, M.: The Shared Socioeconomic Pathways and their
665 energy, land use, and greenhouse gas emissions implications: An overview, *Glob. Environ. Change*, 42, 153–168,
666 <https://doi.org/10.1016/j.gloenvcha.2016.05.009>, 2017.

667 Sander, R.: *Compilation of Henry's Law Constants for Inorganic and Organic Species of Potential Importance in Environmental*
668 *Chemistry*, 1999.

669 Sander, S. P., J. Abbatt, J. R. Barker, J. B. Burkholder, R. R. Friedl, D. M. Golden, R. E. Huie, C. E. Kolb, M. J. Kurylo, G. K.
670 Moortgat, V. L. Orkin, and P. H. Wine: *Chemical Kinetics and Photochemical Data for Use in Atmospheric Studies Evaluation*
671 *No. 17, JPL Publication 10-6, Jet Propulsion Laboratory, Pasadena*, 2011.

672 Schade, G. W. and Goldstein, A. H.: Seasonal measurements of acetone and methanol: Abundances and implications for
673 atmospheric budgets, *Glob. Biogeochem. Cycles*, 20, <https://doi.org/10.1029/2005GB002566>, 2006.

674 Shindell, D. T., Grenfell, J. L., Rind, D., Grewe, V., and Price, C.: Chemistry-climate interactions in the Goddard Institute for
675 Space Studies general circulation model: 1. Tropospheric chemistry model description and evaluation, *J. Geophys. Res.*
676 *Atmospheres*, 106, 8047–8075, <https://doi.org/10.1029/2000JD900704>, 2001.

677 Shindell, D. T., Faluvegi, G., and Bell, N.: Preindustrial-to-present-day radiative forcing by tropospheric ozone from improved
678 simulations with the GISS chemistry-climate GCM, *Atmospheric Chem. Phys.*, 3, 1675–1702, [https://doi.org/10.5194/acp-3-1675-](https://doi.org/10.5194/acp-3-1675-2003)
679 [2003](https://doi.org/10.5194/acp-3-1675-2003), 2003.

680 Singh, H., Chen, Y., Tabazadeh, A., Fukui, Y., Bey, I., Yantosca, R., Jacob, D., Arnold, F., Wohlfrom, K., Atlas, E., Flocke, F.,
681 Blake, D., Blake, N., Heikes, B., Snow, J., Talbot, R., Gregory, G., Sachse, G., Vay, S., and Kondo, Y.: Distribution and fate of
682 selected oxygenated organic species in the troposphere and lower stratosphere over the Atlantic, *J. Geophys. Res. Atmospheres*,
683 105, 3795–3805, <https://doi.org/10.1029/1999JD900779>, 2000.

684 Singh, H. B., O'Hara, D., Herlth, D., Sachse, W., Blake, D. R., Bradshaw, J. D., Kanakidou, M., and Crutzen, P. J.: Acetone in the
685 atmosphere: Distribution, sources, and sinks, *J. Geophys. Res. Atmospheres*, 99, 1805–1819, <https://doi.org/10.1029/93JD00764>,
686 1994.

687 Singh, H. B., Tabazadeh, A., Evans, M. J., Field, B. D., Jacob, D. J., Sachse, G., Crawford, J. H., Shetter, R., and Brune, W. H.:
688 Oxygenated volatile organic chemicals in the oceans: Inferences and implications based on atmospheric observations and air-sea
689 exchange models, *Geophys. Res. Lett.*, 30, <https://doi.org/10.1029/2003GL017933>, 2003.

690 Singh, H. B., Salas, L. J., Chatfield, R. B., Czech, E., Fried, A., Walega, J., Evans, M. J., Field, B. D., Jacob, D. J., Blake, D.,
691 Heikes, B., Talbot, R., Sachse, G., Crawford, J. H., Avery, M. A., Sandholm, S., and Fuelberg, H.: Analysis of the atmospheric
692 distribution, sources, and sinks of oxygenated volatile organic chemicals based on measurements over the Pacific during TRACE-
693 P, *J. Geophys. Res. Atmospheres*, 109, <https://doi.org/10.1029/2003JD003883>, 2004.

694 Solberg, S., Dye, C., Schmidbauer, N., Herzog, A., and Gehrig, R.: Carbonyls and nonmethane hydrocarbons at rural European
695 sites from the mediterranean to the arctic, *J. Atmospheric Chem.*, 25, 33–66, <https://doi.org/10.1007/BF00053285>, 1996.

696 Taylor, K., Williamson, D., and Zwiers, F.: The sea surface temperature and sea ice concentration boundary conditions for AMIP
697 II simulations, PCMDI Report 60, Program for Climate Model Diagnosis and Intercomparison, Lawrence Livermore National
698 Laboratory, 2000.

699 Thompson, C. R., Wofsy, S. C., Prather, M. J., Newman, P. A., Hanisco, T. F., Ryerson, T. B., Fahey, D. W., Apel, E. C., Brock,
700 C. A., Brune, W. H., Froyd, K., Katich, J. M., Nicely, J. M., Peischl, J., Ray, E., Veres, P. R., Wang, S., Allen, H. M., Asher, E.,
701 Bian, H., Blake, D., Bourgeois, I., Budney, J., Bui, T. P., Butler, A., Campuzano-Jost, P., Chang, C., Chin, M., Commane, R.,
702 Correa, G., Crounse, J. D., Daube, B., Dibb, J. E., DiGangi, J. P., Diskin, G. S., Dollner, M., Elkins, J. W., Fiore, A. M., Flynn, C.
703 M., Guo, H., Hall, S. R., Hannun, R. A., Hills, A., Hints, E. J., Hodzic, A., Hornbrook, R. S., Huey, L. G., Jimenez, J. L., Keeling,
704 R. F., Kim, M. J., Kupc, A., Lacey, F., Lait, L. R., Lamarque, J.-F., Liu, J., McKain, K., Meinardi, S., Miller, D. O., Montzka, S.
705 A., Moore, F. L., Morgan, E. J., Murphy, D. M., Murray, L. T., Nault, B. A., Neuman, J. A., Nguyen, L., Gonzalez, Y., Rollins,
706 A., Rosenlof, K., Sargent, M., Schill, G., Schwarz, J. P., Clair, J. M. S., Steenrod, S. D., Stephens, B. B., Strahan, S. E., Strode, S.
707 A., Sweeney, C., Thames, A. B., Ullmann, K., Wagner, N., Weber, R., Weinzierl, B., Wennberg, P. O., Williamson, C. J., Wolfe,
708 G. M., and Zeng, L.: The NASA Atmospheric Tomography (ATom) Mission: Imaging the Chemistry of the Global Atmosphere,
709 *Bull. Am. Meteorol. Soc.*, 103, E761–E790, <https://doi.org/10.1175/BAMS-D-20-0315.1>, 2022.

710 Tsigaridis, K. and Kanakidou, M.: Global modelling of secondary organic aerosol in the troposphere: a sensitivity analysis, *Atmos*
711 *Chem Phys*, 2003.

712 Wang, S., Apel, E. C., Schwantes, R. H., Bates, K. H., Jacob, D. J., Fischer, E. V., Hornbrook, R. S., Hills, A. J., Emmons, L. K.,
713 Pan, L. L., Honomichl, S., Tilmes, S., Lamarque, J.-F., Yang, M., Marandino, C. A., Saltzman, E. S., Bruyn, W. de, Kameyama,
714 S., Tanimoto, H., Omori, Y., Hall, S. R., Ullmann, K., Ryerson, T. B., Thompson, C. R., Peischl, J., Daube, B. C., Commane, R.,
715 McKain, K., Sweeney, C., Thames, A. B., Miller, D. O., Brune, W. H., Diskin, G. S., DiGangi, J. P., and Wofsy, S. C.: Global
716 Atmospheric Budget of Acetone: Air-Sea Exchange and the Contribution to Hydroxyl Radicals, *J. Geophys. Res. Atmospheres*,
717 125, e2020JD032553, <https://doi.org/10.1029/2020JD032553>, 2020.

718 Warneke, C. and de Gouw, J. A.: Organic trace gas composition of the marine boundary layer over the northwest Indian Ocean in
719 April 2000, *Atmos. Environ.*, 35, 5923–5933, [https://doi.org/10.1016/S1352-2310\(01\)00384-3](https://doi.org/10.1016/S1352-2310(01)00384-3), 2001.

720 Weimer, M., Schröter, J., Eckstein, J., Deetz, K., Neumaier, M., Fischbeck, G., Hu, L., Millet, D. B., Rieger, D., Vogel, H., Vogel,
721 B., Reddman, T., Kirner, O., Ruhnke, R., and Braesicke, P.: An emission module for ICON-ART 2.0: implementation and
722 simulations of acetone, *Geosci. Model Dev.*, 10, 2471–2494, <https://doi.org/10.5194/gmd-10-2471-2017>, 2017.

723 Wesely, M. L. and Hicks, B. B.: Some Factors that Affect the Deposition Rates of Sulfur Dioxide and Similar Gases on Vegetation,
724 *J. Air Pollut. Control Assoc.*, 27, 1110–1116, <https://doi.org/10.1080/00022470.1977.10470534>, 1977.

725 Yoshino, A., Nakashima, Y., Miyazaki, K., Kato, S., Suthawaree, J., Shimo, N., Matsunaga, S., Chatani, S., Apel, E., Greenberg,
726 J., Guenther, A., Ueno, H., Sasaki, H., Hoshi, J., Yokota, H., Ishii, K., and Kajii, Y.: Air quality diagnosis from comprehensive
727 observations of total OH reactivity and reactive trace species in urban central Tokyo, *Atmos. Environ.*, 49, 51–59,
728 <https://doi.org/10.1016/j.atmosenv.2011.12.029>, 2012.

729 Yuan, B., Hu, W. W., Shao, M., Wang, M., Chen, W. T., Lu, S. H., Zeng, L. M., and Hu, M.: VOC emissions, evolutions and
730 contributions to SOA formation at a receptor site in eastern China, *Atmospheric Chem. Phys.*, 13, 8815–8832,
731 <https://doi.org/10.5194/acp-13-8815-2013>, 2013.

732 Zhou, X. and Mopper, K.: Apparent partition coefficients of 15 carbonyl compounds between air and seawater and between air
733 and freshwater; implications for air-sea exchange, *Environ. Sci. Technol.*, 24, 1864–1869, <https://doi.org/10.1021/es00082a013>,
734 1990.

